https://doi.org/10.5194/egusphere-2026-2775
Preprint. Discussion started: 27 May 2026

Dust Radiative Effects and Impact on Energy Production over the Mediterranean Basin

Dimitra Kouklaki[1,2], Georgia Charalampous[3,4], Anna Moustaka[5,6], Alkistis Papetta[7], Celia Herrero del Barrio[8,9], Rizos-Theodoros Chadoulis[6], S. Yeşer Aslanoğlu[10], Sara Herrero-Anta[8,9], Michail Mytilinaios[11], Nikolaos Papadimitriou[12], Katerina Anyfanti[12], Christos Spyrou[12], Daniela Meloni[13], Konstantinos Fragkos[7], Yevgeny Derimian[14], Tatiana Di Iorio[15], Rodanthi-Elisavet Mamouri[2,3], Vassilis Amiridis[1], Stavros Solomos[12], Stelios Kazadzis[5], and Ilias Fountoulakis[12]

[1] Institute for Astronomy, Astrophysics, Space Applications and Remote Sensing, National Observatory of Athens, Athens, Greece
[2] Department of Geology and Geoenvironment, National and Kapodistrian University of Athens, Greece
[3] Eratosthenes Centre of Excellence, Limassol, Cyprus
[4] Department of Civil Engineering Geomatics, Cyprus University of Technology, Limassol, Cyprus
[5] Physicalisch Meteorologisches Observatorium, World Radiation Center, Davos, Switzerland
[6] Department of Physics, Aristotle University of Thessaloniki, 54124, Greece
[7] Climate and Atmosphere Research Centre (CARE-C), The Cyprus Institute, Nicosia, Cyprus
[8] Group of Atmospheric Optics (GOA-UVa), Universidad de Valladolid, Valladolid, Spain
[9] Laboratory of Disruptive Interdisciplinary Science (LaDIS), Universidad de Valladolid, Valladolid, Spain
[10] Department of Environmental Engineering, Hacettepe University, Ankara, Türkiye
[11] Consiglio Nazionale delle Ricerche - Istituto di Metodologie per l'Analisi Ambientale (CNR-IMAA), Tito, Italy
[12] Research Centre for Atmospheric Physics and Climatology of the Academy of Athens, Greece
[13] Sustainable Department, National Agency for New Technologies, Energy and Sustainable Economic Development, Rome, Italy
[14] Univ. Lille, CNRS, UMR 8518 - LOA - Laboratoire d'Optique Atmosphérique, F-59000 Lille, France
[15] Laboratory for Models and Measurements for Air Quality and Climate Observations, ENEA, Rome, Italy

Correspondence to: Dimitra Kouklaki (d.kouklaki@noa.gr)

Abstract. Atmospheric aerosols are among the key factors affecting the Earth's radiation budget, playing a fundamental role in understanding climate forcing, feedback mechanisms, and their impact on future climate projections and on solar energy systems. More specifically, dust aerosol particles, which are characterized by high complexity of their optical and microphysical properties, remain one of the most uncertain components. In this study, we focus on four severe dust events across multiple sites in the broader Mediterranean Basin between 2021 and 2022. We employ a combination of ground-based remote sensing observations along with Radiative Transfer (RT) modelling, with the libRadtran package and METAL-WRF scheme, as well as photovoltaic (PV) power generation simulations using the Global Solar Energy Estimator (GSEE) to investigate the impact of the different optical and geometrical aspects of these events on solar radiation and solar energy. The results revealed that the strongest dust-induced attenuation was systematically observed in the direct component of solar radiation (DNI), with maximum losses frequently exceeding 60–80%, while Global Horizontal Irradiance (GHI) typically ranged between 5% and 25%. These findings were reflected directly into substantial PV power output losses, for both fixed-tilt and two-axis tracking systems, reaching ~45% and 80%, respectively, with the impact on the latter being significantly

https://doi.org/10.5194/egusphere-2026-2775
Preprint. Discussion started: 27 May 2026

higher due to their strong dependence on DNI. A sensitivity analysis based on how aerosol optical properties and solar geometry jointly influence PV energy production revealed that Solar Zenith Angle (SZA) plays the most dominant role, followed by Aerosol Optical Depth (AOD), which leads to strong attenuation independently of SZA under altered aerosol load conditions. Finally, the comparison of the modelled PV output estimated from the modelled irradiances based on the two different RT models with the PV output considering ground-based GHI measurements revealed a similar agreement under clear sky conditions, while under cloudy conditions, the analysis revealed the critical role of the diffuse horizontal irradiance (DHI) component in the simulations.

1 Introduction

Recent advancements in renewable energy have underscored the vital role of solar power in the global energy transition. Notably, solar and wind energy have become pivotal to global electricity generation according to the International Renewable Energy Agency (IRENA, 2023). More specifically, solar photovoltaic (PV) systems are becoming an essential solution to meet the ever-increasing electricity demand, with installations across the Saharan desert among the largest worldwide (Benban, Egypt, with PV systems and Ouarzazate Solar Power Station in Morocco for concentrated solar power (CSP) installations). However, large-scale climate variations on continental and decadal scales present significant challenges to the long-term availability of solar resources (Engeland et al., 2017). As a result, understanding the atmospheric conditions that affect solar energy production has gained significant attention in recent years. A crucial climate variable and an essential determinant that governs solar energy production (Müller et al., 2014) is the downward shortwave (SW) radiation, which represents the amount of solar radiation reaching the Earth's surface. Incoming SW radiation is strongly dependent on variable atmospheric parameters (mainly clouds and aerosols, e.g., Wild et al., 2017, Kazadzis et al., 2018), which, in turn, affect solar energy availability and efficiency. Among these, atmospheric aerosols are one of the most significant influencing factors, especially under clear-sky conditions.

Atmospheric aerosols, and more precisely dust particles, can have large environmental, health, and socio-economic impacts far from their source regions (Monteiro et al., 2022). The effects of aerosols on climate are generally classified as direct and indirect (Lohmann and Feichter, 2001; Forkel et al., 2012; Haywood and Boucher, 2000). Dust particles can significantly impact regional atmospheric circulation and the radiation budget at both the surface and in the atmosphere. Depending on their optical and microphysical properties, dust aerosols act as a regulator of surface solar radiation (SSR) by directly absorbing or scattering it (Li et al., 2022), known as the direct radiative effect (DRE) (Li et al., 2004; Biagio et al., 2020) and indirectly affecting the number of cloud condensation nuclei (CCN) particles and precipitation (Twomey, 1991; Ramanathan et al. 2001; Boucher 2015). More specifically, smaller dust particles primarily scatter SW radiation, while larger particles absorb it, leading to a cooling and a warming effect, respectively. Based on regional studies across Europe and the Mediterranean (Ruckstuhl et al., 2010; Nabat et al., 2015; Drugé et al., 2019), shifts in aerosols have been identified as a key driver of global SSR changes, indicating a strong relation to aerosol variability.

https://doi.org/10.5194/egusphere-2026-2775
Preprint. Discussion started: 27 May 2026

However, critical gaps in dust observation have not yet been fully identified. Dust observation systems provide the opportunity to identify and contribute to the improvement of dust monitoring and forecast models (Mona et al., 2023). Substantial gaps still remain in robustly constraining uncertainties in dust radiative forcing, and specifically those stemming from source-region variability, propagated into dust impacts on both SW and longwave (LW) radiative balance (Kok et al., 2021). More precisely, the global mean SW DRE was estimated to be approximately -0.40 W/m^2 (with the 90% confidence range between -0.10 and -0.70 W/m^2) while the LW DRE was estimated at +0.25 W/m^2 (with a range of +0.10 and +0.40 W/m^2) (Kok et al., 2023).

Dust Optical Depth (DOD), as part of the total aerosol optical depth (AOD), represents the overall effect of dust on the direct solar irradiance and is generally considered the most important parameter regarding the direct radiative effects of dust (e.g., Li et al., 2021; Gkikas et al., 2021; 2022). Nevertheless, even if DOD at a specific wavelength remains constant during different dust events, other optical and microphysical properties such as the Ångström exponent (AE) and the single scattering albedo (SSA) can have a very significant impact not only on the absolute SSR levels, but also on its spectral composition, as well as on its distribution in the sky (e.g., Che et al., 2018; Fountoulakis et al., 2024), inducing biases in the DRE and the overall radiative forcing estimates. These properties depend strongly on dust origin (e.g., Rodriguez et al., 2020), as well as the interaction of different types of aerosols and pollutants (e.g., Teri et al., 2025).

SSA depends on the overall composition of the aerosol mixture, and in the case of dust particles, it decreases with increasing particle size. More precisely, submicron particles reach SSA values close to 1, while supermicron dust is characterized by lower SSA values (Adebiyi et al., 2022), indicating the absorption of a substantial amount of radiation. SSA is influenced by the complex refractive index, which is determined by the mineral composition of dust particles and is wavelength dependent (Sokolik et al., 1999).

The large spatiotemporal heterogeneity of dust sources (Uno et al., 2009; Francis et al., 2020) results in correspondingly large variability in dust mineralogical properties, and subsequently large variations in the absorptivity of dust layers. In addition, dust particles can be conveyed far from their sources (Gkikas et al., 2013, 2015, 2016; Flaounas et al. 2015; Marinou et al, 2017; Aslanoğlu et al., 2022), which also leads to the modification of their already complex and challenging composition (Seinfeld et al., 2004; Denjean et al., 2016; Renard et al., 2018; Riemer et al., 2019; Go et al., 2022; Mateos et al., 2026). Therefore, accurate data on the spatial and temporal variability of dust optical properties is essential for estimating dust-induced DREs (Samset et al., 2018) and, finally, their impact on PV power potential (Kosmopoulos et al., 2017, 2018; Rezvani et al., 2023; Papadimitriou et al., 2026).

The Mediterranean Basin is one of the most vulnerable regions to environmental change, experiencing severe seasonal dust transport (e.g., Gómez-Amo et al., 2011), significantly altering its aerosol burden and radiative balance. Most of the dust layers reaching the Mediterranean region originate from North Africa and the Arabian Peninsula - areas that host some of the most active dust sources globally, contributing to nearly 80% of global dust emissions (Kok et al., 2021; Warren et al., 2007). Substantial emissions also arise from the western Sahara, the eastern Libyan Desert, and the Nubian Desert (Engelstaedter et al., 2006). Similarly, the Arabian Peninsula is a major source region for mineral dust aerosols (Jish Prakash et al. 2015; Middleton, 1986). Changes in the frequency, the severity, and the extent of dust events have been recorded in the last few

https://doi.org/10.5194/egusphere-2026-2775
Preprint. Discussion started: 27 May 2026

decades due to changing atmospheric conditions. Intensifying drought, desertification, and changing atmospheric circulation patterns would result in further increases in the future (e.g., Rodríguez et al., 2024; Cuevas et al., 2024; Abadi et al., 2025). Such increases in dust activity are expected to modulate its radiative effects. Recent studies have highlighted that higher dust loads can significantly influence the global radiative forcing (Kok et al., 2023; Haugvaldstad et al., 2025), with historical simulations indicating that higher dust loads can increase global mean cooling even up to 40% (Leung et al., 2025).

The extensive transport of dust over the Mediterranean Basin can cause significant changes in the performance of solar power systems by diminishing the output of the PV panels (Ruiz-Arias et al., 2006) and the CSP systems (Muller et al., 2014; Polo et al., 2015). More precisely, PV systems are mostly affected by variations in Global Horizontal Irradiance (GHI) while CSP efficiency relies mostly on Direct Normal Irradiance (DNI). Given that the Mediterranean Basin is among the sunniest regions of our planet with long insolation hours, the role of aerosols, and especially dust, is comparable to - and over specific regions dominant over - the role of clouds (e.g., Kosmopoulos et al., 2018; Fountoulakis et al., 2021). Dust's dominant role in attenuating solar irradiance poses a serious challenge to solar power generation (Meloni et al., 2004; Gómez-Amo et al., 2011; Antón et al., 2012; IEA, 2023). Several studies have been conducted focusing on understanding DRE (e.g., Pérez et al., 2006; Nabat et al., 2015; Gkikas et al., 2018; Fountoulakis et al., 2021; 2024; Papachristopoulou et al., 2022; Masoom et al., 2023) and the effect on solar energy (e.g., Gómez-Amo et al., 2019; Alonso-Montesinos et al., 2020; Kouklaki et al., 2023). Neher et al. (2019) revealed significant reductions in PV output due to dust storms, of up to 79% on a daily basis, while Kosmopoulos et al. (2017) estimated that the attenuation of an extreme dust event can reach 40–50 % in the case of GHI and a much stronger DNI decrease of approximately 80–90 %, highlighting the significant effect of such events on solar energy production. In a more recent study, Varga et al. (2026) showed that Saharan dust events reduce PV output on a national level at the Mediterranean countries by an average of 25–40%, with losses exceeding 50% during extreme events.

The variability in dust aerosol emission intensity, timing, and mineral composition across regions adds considerable complexity and uncertainty in assessing dust-climate interactions, while the spatio-temporal heterogeneity makes it even more complex to account for in climate models. Accurate knowledge of these source-dependent characteristics is essential to quantify the dust DRE with confidence. Observational data, such as in-situ measurements and remote sensing observations from ground-based and satellite platforms, are crucial for improving dust parameterizations and enhancing our understanding of these processes and, finally, the dust effect on SSR and climate.

Our study aims to evaluate the impact of atmospheric dust on solar radiation and PV energy production potential over the Mediterranean Basin. Previous work by Papetta et al. (2026) has extensively analyzed data from several AERONET (AErosol RObotic NETwork) stations across the Mediterranean Basin located in regions that have experienced significant dust events during the period 2021-2022. Essential measured dust optical properties have been employed along with back-trajectory models to identify the geographic origin of dust in each case, allowing us to link observed radiative effects to source-specific characteristics. Based on the same events, we quantified the impact of dust on the levels of the SSR through Radiative Transfer (RT) modeling and assessed its implications for PV system performance and solar energy production. Furthermore, we quantified the sensitivity of PV output to the variability in dust optical properties such as AOD, AE, and SSA across the range

https://doi.org/10.5194/egusphere-2026-2775
Preprint. Discussion started: 27 May 2026

of values observed during the afore-mentioned intense dust events. Finally, we discuss how differences between dust optical properties as measured by AERONET and those considered by the METAL-WRF model are affecting the modelled PV output during intense dust events.

This paper is outlined as follows: The introduction is provided in Section 1, followed by the methodology used to collect and analyze data, described in Section 2. Analysis and discussion of the results are presented in Section 3. Finally, the main findings of the study are summarized in Section 4, along with suggestions for further analysis.

2 Data and Methodology

This section outlines the methodology followed to assess the radiative effects of dust and their impact on solar energy production over the Mediterranean Basin. We present the observational datasets and modeling tools employed, along with the criteria and procedures used to identify representative dust events. The analysis combined ground-based measurements, RT simulations, and energy system models with view to quantifying changes in solar radiation and photovoltaic performance.

2.1 AERONET

AERONET is a global network of ground-based sun-photometers that measure atmospheric aerosol properties (Holben et al., 1998). Cimel CE318, the standard instrument of AERONET, measures direct sun and sky radiances at a number of fixed wavelengths within the visible and near-infrared (VNIR) spectrum to retrieve columnar aerosol optical properties. More precisely, AERONET provides continuous cloud-screened observations of spectral AOD, precipitable water, and inversion aerosol products in diverse aerosol regimes. Inversion products are retrieved from sky radiance measurements performed with different viewing geometries (Dubovik and King, 2000). Together with AOD, these measurements provide inputs for inversion algorithms to derive essential aerosol microphysical and radiative properties such as volume size distribution, refractive index, SSA, and scattering phase function.

In the frame of this study, Level 1.5 Version 3.0 (Giles et al., 2019) AERONET products from the retrieval algorithm were employed for the under-study dust events. More specifically, AOD along with AE, SSA, Asymmetry Parameter (ASY), and Precipitable water (PW) were used. To further ensure the reliability of aerosol retrievals and minimize potential cloud contamination, we considered only measurements with a sky residual parameter < 5%.

2.2 Selection of dust events

The dust events across the Mediterranean Basin, which form the primary focus of this study, were identified through AERONET observations collected from all monitoring stations in the region. As a first step, the dust episodes were identified relying on two main criteria: (i) AOD at 500nm >0.2 and (ii) AE at 380-500nm <0.3. In addition, IASI and MODIS satellite AOD data (Callewaert et al., 2019), as well as MIDAS (Gkikas et al., 2021) and LIVAS (Amiridis et al., 2015) climatological data were used to confirm the presence of mineral dust particles in the atmosphere. Spatial maps were generated based on these

https://doi.org/10.5194/egusphere-2026-2775
Preprint. Discussion started: 27 May 2026

thresholds to detect 20-day intervals in which dust affected more than 10 AERONET stations, allowing the identification of widespread dust activity across the region. Slightly more flexible criteria were used for the identification of dust events originating from the Middle East (at least 6 impacted sites, AE<0.5). These modified criteria were applied because (1) fewer AERONET stations were at the transfer path of dust, and (2) we noticed that AE during dust events from the Middle East was generally larger than 0.3, possibly due to the presence of smaller particles in the aerosol mixture when dust originates from the Middle East.

A detailed analysis was conducted to identify representative stations, ensuring broad spatial coverage of the region, with priority given to those with available inversion and vertical profile data from lidar or ceilometer observations. For periods when multiple sub-events occurred, only the most intense was considered.

Furthermore, the arrival height of the dust plumes was estimated from co-located vertical profile observations from ground-based lidars, when available (e.g., from the Aerosol, Clouds and Trace Gases Research Infrastructure and the European Aerosol Research Lidar Network (ACTRIS/EARLINET; Pappalardo et al., 2014). Considering this information, the performance of HYSPLIT (Stein et al., 2015) back-trajectory analysis for the representative stations enabled the confirmation of the sources and transport pathways of the dust plumes.

While the present study focuses on the radiative effect during these dust events, it is important to note that, as shown in Papetta et al. (2026), although dust is the dominant species in the aerosol mixture for the studied cases, other aerosol species coexist with dust and affect the effective optical properties that are measured by AERONET. Thus, the presented results correspond to the attenuation of SSR during intense dust events, also considering the role of other pollutants that are either local or are being mixed with dust as it is transferred over the sites of the measurements.

An extended description of the afore-mentioned selected events and the respective analysis on the aerosol properties is given in (Papetta et al., 2026). The periods and AERONET station locations affected during the selected dust events for which the investigation is conducted are presented in Table 1.

Event A	**Event B**	**Event C**	**Event D**
18 – 29 March 2021	**17 – 28 June 2021**	**10 – 21 November 2021**	**21 April – 1 May 2022**
Antikythera	Antikythera	Sede Boker	Lampedusa
Cairo	Athens	Weizmann Institute	Mallorca
Finokalia	Ben Salem	Cairo	Rome
Nicosia	Rome	Agia Marina Xyliatou	Valladolid
Sede Boker	Magurele-Inoe	IMS-METU-ERDEMLI	Athens
CUT-TEPAK	Thessaloniki	Finokalia	CUT-TEPAK

Table 1: The locations and periods of the four selected dust events that occurred during the period 2021-2022 in the Mediterranean Basin.

https://doi.org/10.5194/egusphere-2026-2775
Preprint. Discussion started: 27 May 2026

2.3 Radiative Transfer Model Simulations

Towards estimating the radiative effect of the selected dust events over the afore-mentioned ground-based stations, we performed RT simulations utilizing the uvspec model of the libRadtran package (Mayer and Kylling, 2005; Emde et al., 2016). To solve the radiative transfer equations, the DIScrete Ordinates Radiative Transfer (DISORT) solver was employed (Stamnes et al., 1988, 2000; Buras et al., 2011). The RT calculations were performed in the SW spectral range of 280-3000 nm, relevant to the spectral range of PV systems, using a 16-stream pseudospherical approximation exploiting the extraterrestrial solar spectrum with a 1.0 nm step suggested by Kurucz et al. (1992). The scattering and absorption of solar radiation from atmospheric gases and aerosols, as well as the reflectance of the Earth's surface, were also taken into consideration in the RT simulations. Regarding the molecular absorption, the REPresentative wavelength radiative TRANsfer method (REPTRAN; Buehler et al., 2010; Gasteiger et al., 2014) was employed in the default spectral resolution of 15 cm^{-1}.

The standard US atmospheric profile (Anderson et al., 1986) was utilized for all simulations to parametrize the trace gas concentrations, in which the default profiles of ozone (TCO), water vapor (TCWV), and carbon dioxide (TCCO2) were scaled to explicitly defined columnar values. More precisely, TCWV was adjusted with AERONET PW retrievals while constant climatological values of 410 ppm for CO2 and 300 DU for O3 concentrations were set. Solar zenith angle (SZA) and the location coordinates were also provided for each station. The datasets regarding the aerosol and other atmospheric parameters for each station were provided at half-hour intervals, which was selected to be the frequency of the RT simulations in order to produce a complete daily dataset. Finally, the surface albedo was set to 0.2 for all simulations.

To investigate the dust radiative effects, simulations were performed for two configurations (a) separately for the two spectral regions 280 – 500 nm and 500 – 3000 nm, based on realistic aerosol inputs (Section 2.4) and for (b) the total wavelength range of 280 – 3000 nm, for which a sensitivity analysis was performed regarding the different input parameters (Section 2.5). Finally, the broadband SW GHI and DNI at the bottom of the atmosphere (BOA), considering clear-sky (cloudless) conditions, were calculated in order to further investigate the effect of the different dust events on solar energy production from PV panels. A flowchart illustrating the above-mentioned methodology is presented in Fig. 1.

https://doi.org/10.5194/egusphere-2026-2775
Preprint. Discussion started: 27 May 2026

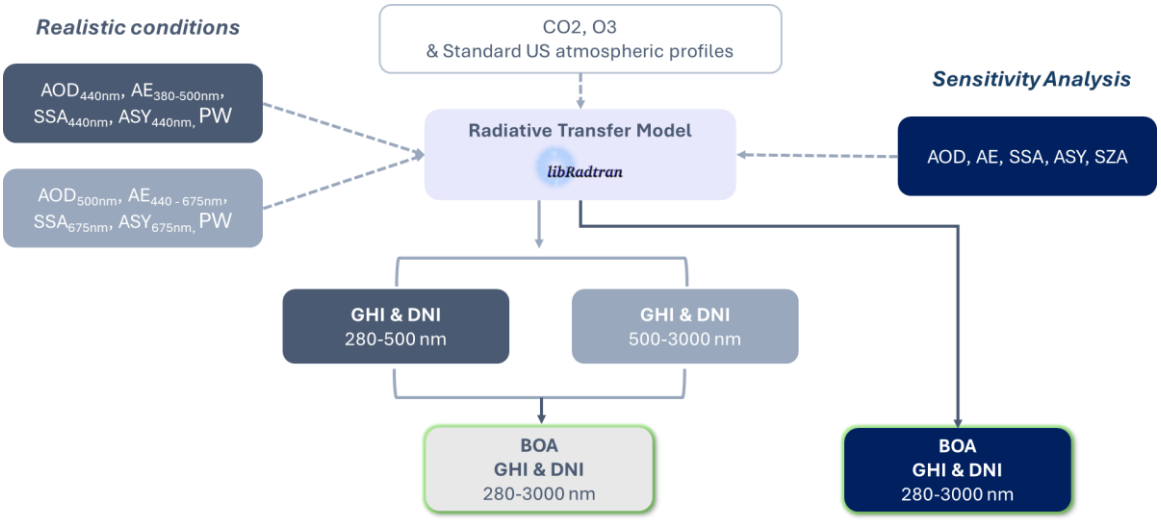

Figure 1: Flowchart of the methodology followed for the assessment of the aerosol radiative effect based on AERONET products during severe dust events in the Mediterranean Basin and the effect of the most essential aerosol properties on solar radiation through a sensitivity analysis.

2.4 Quantification of the effect of dust

A first set of simulations was performed with realistic aerosol optical properties (AOD, AE, SSA, and ASY) and other atmospheric parameters (e.g., PW) acquired from the AERONET database, as described in Section 2.2. The aerosol properties in the RT simulations for the two spectral areas (280 – 500 nm and 500 – 3000 nm) were provided at two different wavelengths, with respect to the spectral range.

In the ultraviolet (UV)-visible range (280-500 nm), AOD, SSA, and ASY retrieved at 440 nm were assumed to be representative and were therefore used in the simulations, while in the visible-near-infrared range (500-3000 nm), AOD at 500nm and SSA and ASY at 675 nm were applied. The spectral dependence of AOD was accounted for by using the AE over 380-500nm and 440-675 nm for the respective spectral intervals. Additional atmospheric parameters were specified to better represent the atmospheric conditions, with CO2 set to 410 ppm and O3 to 300 DU in all cases.

The different spectral bands of the simulations aimed to capture the effect of the spectrally dependent aerosol optical properties. As previously shown in several studies (e.g., Kazadzis et al., 2016; Mok et al., 2018; Fountoulakis et al., 2019; Papetta et al., 2026), ASY and SSA generally exhibit greater spectral dependence at wavelengths below 500 nm. A more accurate representation of the spectral variability of these properties would demand measurements with a finer spectral resolution at the full range of the spectral simulations. Such measurements are available at very few stations globally. Given that the most commonly used types of panels are sensitive at wavelengths shorter than approximately 1200 nm (Senthilarasu et al., 2015; Kouklaki et al., 2023), uncertainties due to the inaccurate description of aerosol properties at such wavelengths are not as significant as the uncertainties at shorter wavelengths.

https://doi.org/10.5194/egusphere-2026-2775
Preprint. Discussion started: 27 May 2026

Finally, to quantify the dust radiative effect, the RT simulations were repeated for aerosol-free atmospheric conditions, remaining the rest of the atmospheric conditions unchanged with respect to the initial setup (e.g., PW, CO2, and O3). The radiative impact of the local (dust-dominated) aerosol mixtures was estimated through the comparison between the SSR for sky conditions with aerosol load and pristine sky conditions.

2.5 Sensitivity analysis

Towards the quantification of the impact of dust on PV power potential due to the attenuation of the SSR, we conducted a sensitivity analysis to investigate how different dust optical properties, within the range of measurements during the selected events, affect energy production. The sensitivity relied on different input parameters (AOD, AE, SSA, ASY, and SZA) in the simulations, which are presented in Table 2. Therefore, to account only for the effect of these specifically defined parameters, the water vapor was derived from the US-standard atmosphere profile in all simulations.

The RT simulations in this case were performed for the total wavelength range of 280 – 3000 nm. Additionally, to save computational time from time-expensive line-by-line calculations of spectral molecular absorption, the sufficiently accurate band parameterization of correlated-k KATO distribution (Kato et al., 1999) was used.

Parameter	Range	Step
AOD	0-1.6	0.1
AE	0-0.4	0.2
SSA	0.84-0.99	0.03
ASY	0.62-0.82	0.04
SZA	0-75°	15°

Table 2: Sensitivity analysis input parameters along with the range of their values and the respective steps that were used in the RT simulations.

2.6 The GSEE model

The PV power generation simulations were conducted using the Global Solar Energy Estimator (GSEE; Pfenninger & Staffel, 2016). The model includes modules that enable the simulation of a complete PV system, incorporating parameters such as the installed capacity, technology (c-Si, CdTe), tracking (fixed, 1- or 2-axis), tilt angle, and azimuth orientation. The user specifies the coordinates of the project location and provides as input a time series of solar radiation data, and optionally, ambient temperature and surface albedo.

In our simulations, we defined PV plants using both available panel technologies and for the mounting approach, either fixed or 2-axis tracking. For fixed panels, the tilt angles were calculated using the built-in latitude linear function included in the

https://doi.org/10.5194/egusphere-2026-2775
Preprint. Discussion started: 27 May 2026

model, considering also a south orientation of the PV panels. Moreover, we calculated the energy production per unit of nominal capacity (1 kWp).

2.7 The METAL-WRF model

The METAL-WRF system reproduces the relative abundances of the various dust minerals in the atmosphere (Solomos et al., 2023). This is accomplished by coupling the GOCART-AFWA dust emission scheme with prognostic tracers for nine mineral species -illite, kaolinite, smectite, calcite, quartz, feldspar, hematite, gypsum, and phosphorus- as well as iron. Mineral composition data for source regions are derived from the high-resolution GMINER30 (Nickovic et al., 2012) and FERRUM30 (Nickovic et al., 2013) databases. The system simulates the full life cycle of each mineral, accounting for transport, gravitational settling, and a specialized wet-scavenging module developed specifically for the mineral atmospheric life cycle as described in Solomos et al., 2023. As a result, the model produces spatially explicit fields of mineral-specific dust mass, which we use to identify source signatures and track their evolution during transport across the Mediterranean.

In METAL-WRF, aerosol optical properties are computed by combining mineral-resolved dust mass concentrations with wavelength-dependent refractive indices. Optical parameters (extinction, SSA, asymmetry factor) are diagnosed using Mie-based lookup tables and passed to the Rapid Radiation Transfer Model for GCM (RRTMG; Mlawer et al., 2016; Mlawer et al., 1997; Mlawer and Clough,1998) to calculate aerosol radiative forcing.

Recently, the METAL-WRF model has been upgraded to incorporate the direct radiative impact of the minerals in dust. The radiative transfer scheme of METAL-WRF has recently been validated in recent work by Spyrou et al. (2025) and revealed good agreement between the model and the measurements. In this work, we compare the PV power potential as it has been estimated by coupling the GSEE model with libRadtran simulations and the METAL-WRF GHI output, for the dust event of April - May 2022.

2.8 Uncertainties

The results presented in this paper are mainly affected by uncertainties in radiative transfer modelling and uncertainties in solar power potential modelling.

Uncertainties related to radiative transfer (RT) modelling: Uncertainty in RT simulations lies mostly in the uncertainty in the input parameters (Schwander et al., 1997; Weihs and Webb, 1997). Uncertainties in the used AERONET AOD values are ~ 0.01 (VIS) - 0.02 (UV) (Giles et al., 2019; Sinyuk et al., 2020), while the use of AE at specific wavelength bands adds more uncertainty in the parameterization of AOD since AE does not capture the AOD spectral behaviour perfectly, especially at wavelengths that are outside of the considered AE ranges (e.g., shorter UV wavelengths as discussed in Kazadzis et al., 2016). Overall, these latter uncertainties are less significant in the calculation of the GHI and DNI integrals. Another significant uncertainty factor in RT modelling is the spectral description of the SSA. Uncertainties in AERONET SSA retrievals are of the order of 0.03 for AOD values (at 440 nm) exceeding 0.4 (Dubovik et al., 2000). However, using a fixed SSA value (SSA at 440 nm) for the simulations at wavelengths below 500 nm introduces more uncertainties, since for dust, SSA decreases fast

https://doi.org/10.5194/egusphere-2026-2775
Preprint. Discussion started: 27 May 2026

with decreasing wavelength in the UV spectral region (e.g., Kazadzis et al., 2016). The latter assumption results in uncertainties, especially regarding the ratio between the diffuse and direct components of the irradiance, as moving from the VIS to the UV-B region. Nevertheless, the contribution of very short UV-B wavelengths to the DHI and DNI integrals is relatively small, taking into account the small contribution of UV wavelengths in the VIS region. Uncertainties in the used asymmetry parameter are generally less impactful on the retrieved irradiances relative to uncertainties in AOD and SSA. Similarly, uncertainties in the used aerosol and atmospheric properties profiles are also estimated to be within the overall uncertainty budget of the RT simulations due to the factors discussed above (see e.g., Fountoulakis et al., 2022). An accurate quantification of all the aforementioned would need a lot of effort and is outside the scope of this study.

Uncertainties related to PV power potential modelling: GSEE models the solar power potential, i.e., the maximum level of energy that can be produced by a specific type of solar panel. Uncertainties in the simulated PV power potential depend primarily on the input irradiances. If both components (direct/diffuse) are known, then uncertainties arise from the fact that the model assumes a standard geometry for the diffuse irradiance, i.e., uses a simple isotropic-type assumption when converting irradiance to the plane of the array. Depending on the atmospheric composition, however, the distribution of the diffuse radiation in the sky changes, resulting in photons reaching the panels from different directions, which changes the efficiency of the diffuse component to produce energy. If only GHI is known, then the distribution in its two components is estimated using Boland-Ridley-Lauret (BRL; e.g., Lauret et al., 2013), which introduces further uncertainties, especially under intense dust events. According to Papadimitriou et al. (2026), the ratio between the diffuse component and GHI can decrease by ~ 0.4 (relative to its initial value) when retrieved from BRL for a dust optical depth of ~ 1. Furthermore, GSEE considers a fixed relationship between the total amount of the two solar irradiance components and their spectral composition. Obviously, spectral composition changes depending on atmospheric compositions (e.g., in the presence of small reflective aerosol particles, the contribution of shorter wavelengths in the diffuse component of solar radiation is increased). It is also impossible to parameterize the exact temperature of the different components of a PV installation. Using the ambient temperature as a proxy for the GSEE simulations also adds uncertainties. Since the bibliography is poor regarding the impact of the aforementioned factors, it is not easy to make, even a rough estimation of the overall uncertainty budget. More uncertainties arise if we try to model the actual power production (instead of the power production potential) since factors such as soiling on the panels, module performance parameters, system losses, uncertainties related to panel orientation, etc., can also play a significant role (e.g., Thevenard and Pelland, 2013; Sepúlveda-Oviedo, 2025).

3 Results and discussion

3.1 Dust effect on the levels of surface solar radiation (GHI, DNI) and PV output

Our analysis across the four selected dust events (March 2021, June 2021, November 2021, and April 2022) revealed a consistent reduction in surface solar radiation and corresponding PV output across all Mediterranean and Middle Eastern stations.

https://doi.org/10.5194/egusphere-2026-2775
Preprint. Discussion started: 27 May 2026

The strongest dust-induced attenuation was systematically observed in the direct component of solar radiation (DNI), with maximum losses frequently exceeding 60–80% during intense dust episodes (Fig. 2a). Stations located closer to major dust source regions or along dominant transport pathways (such as SEDE_BOKER, Cairo_EMA_2, CUT-TEPAK, and Ben_Salem) experienced the most severe reductions, particularly during March 2021 and June 2021 events. This denotes that a decrease in DNI reflects the strong extinction of the direct solar beam by mineral dust through a combination of scattering and absorption processes, which becomes increasingly efficient as dust optical depth increases. In contrast, GHI exhibited more moderate reductions, typically ranging between 5% and 25% across most of the stations (Fig. 2b). This behaviour highlights the compensating role of the diffuse radiation component under dusty conditions, whereby part of the attenuated direct radiation is redistributed into the diffuse field, partially offsetting total GHI losses.

The afore-mentioned combined radiative effects were reflected directly into substantial reductions in PV power output (Fig. 3). For fixed-tilt PV systems (Tracking = 0, Fig. 3a), maximum daily power losses typically ranged between 10% and 45%, depending on station location and event intensity. Observed losses were systematically higher during March and June 2021 events, in agreement with the elevated dust loads and stronger DNI attenuation observed during these periods. For two-axis tracking systems (Tracking = 2, Fig. 3b), PV power losses were significantly amplified, frequently exceeding 50–80% at stations strongly affected by dust intrusions. This pronounced sensitivity arises from the strong dependence of tracking systems on the direct solar component, which is disproportionately reduced during dust events. Consequently, although tracking systems generally outperform fixed installations under clear-sky conditions, their relative vulnerability to intense dust episodes becomes evident during high-AOD conditions.

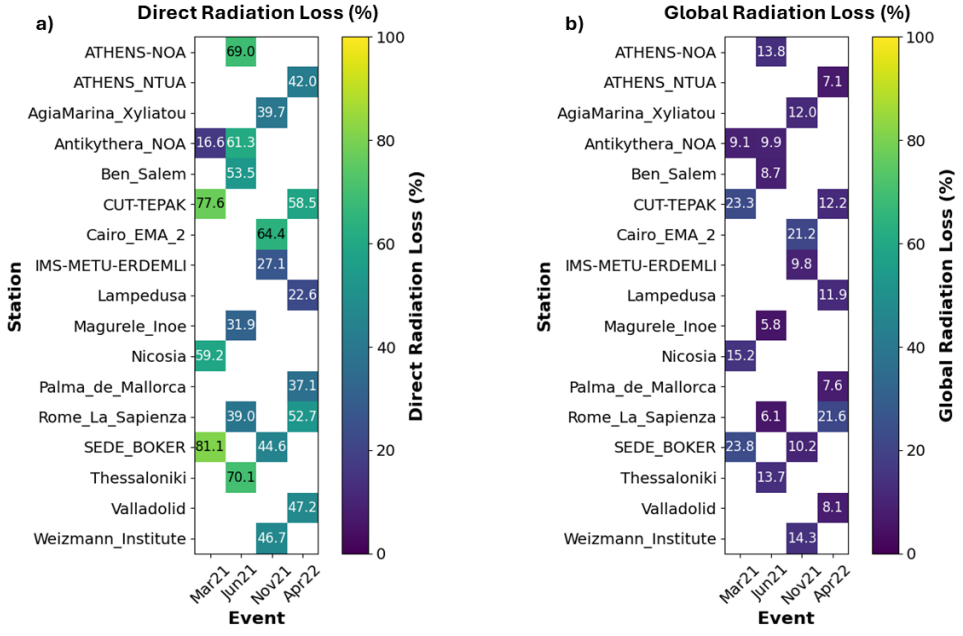

Figure 2: Heatmaps of direct (a) and global (b) radiation loss (%) during four major dust events (March 2021, June 2021, November 2021, and April 2022) across multiple monitoring stations in the Mediterranean and Middle East.

https://doi.org/10.5194/egusphere-2026-2775
Preprint. Discussion started: 27 May 2026

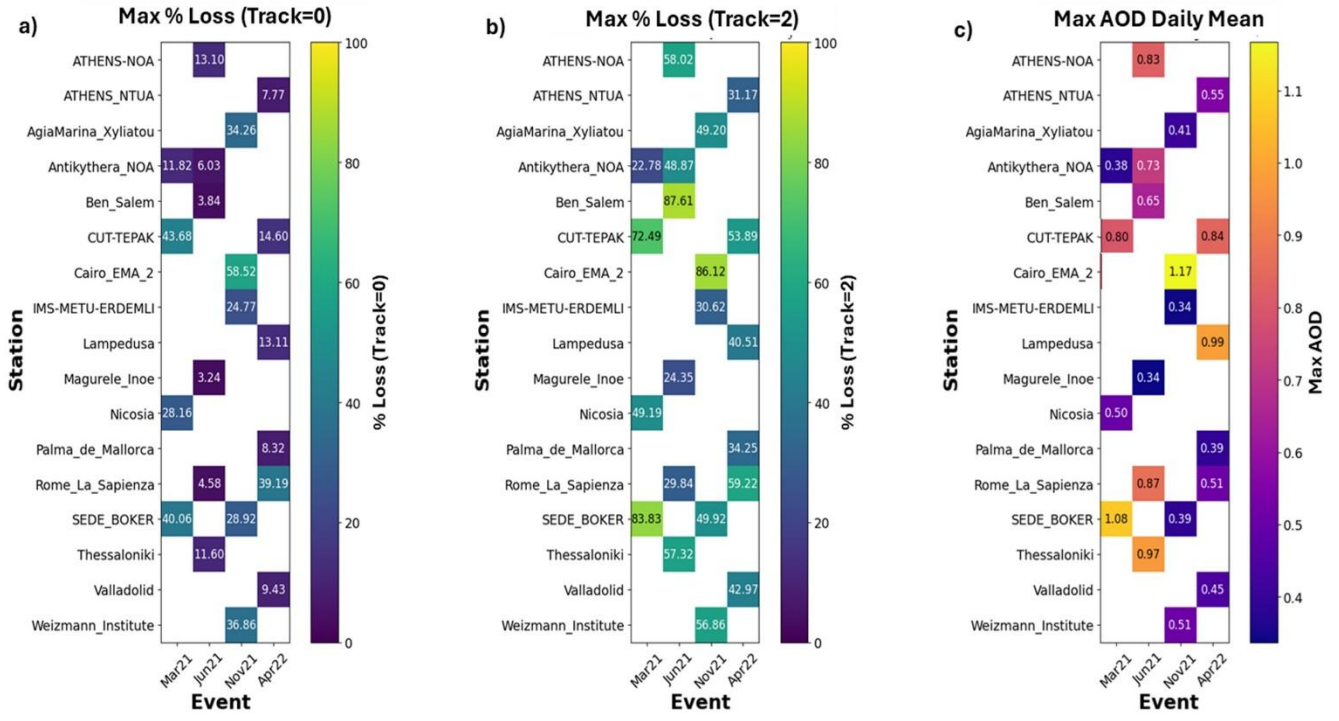

Figure 3: Losses (in %) in produced solar energy in the day of the maximum (daily average) AOD a) for fixed-tilt PV systems (Tracking = 0), two-axis tracking systems (Tracking = 2), along with c) the maximum observed (daily average) AOD values.

To further investigate the relationship between solar energy losses and the corresponding global and direct radiation losses, we directly compared the findings presented in Figs. 2 and 3 for both fixed-tilt and two-axis tracking systems. The analysis incorporates all events with respect to the respective maximum (daily average) AOD (Fig. 3c) to identify differences in system performance due to changing atmospheric conditions. Overall, the afore-mentioned comparison (Fig. 4) demonstrates a consistent relationship between solar energy and radiation losses, for both the global and direct components. More precisely, solar energy losses increased systematically for both system configurations with increasing radiation losses, as expected, since radiative attenuation is the primary driver of PV performance degradation under these conditions. In the case of direct irradiance, this effect is more pronounced (exhibiting losses of up to ~80%, corresponding to approximately 55% higher than global radiation losses), indicating a tighter dependence than that of the diffuse component. Additionally, increasing AOD is consistently associated with higher losses in radiation and, therefore, energy, while the observed residual variability suggests that other parameters might also be associated with these observations. Finally, two-axis PV tracking systems exhibit higher solar energy losses for comparable radiation attenuation than fixed-tilt systems, reflecting their sensitivity to these effects, and more precisely their stronger dependence on the direct irradiance under high aerosol loading conditions in the atmosphere.

https://doi.org/10.5194/egusphere-2026-2775
Preprint. Discussion started: 27 May 2026

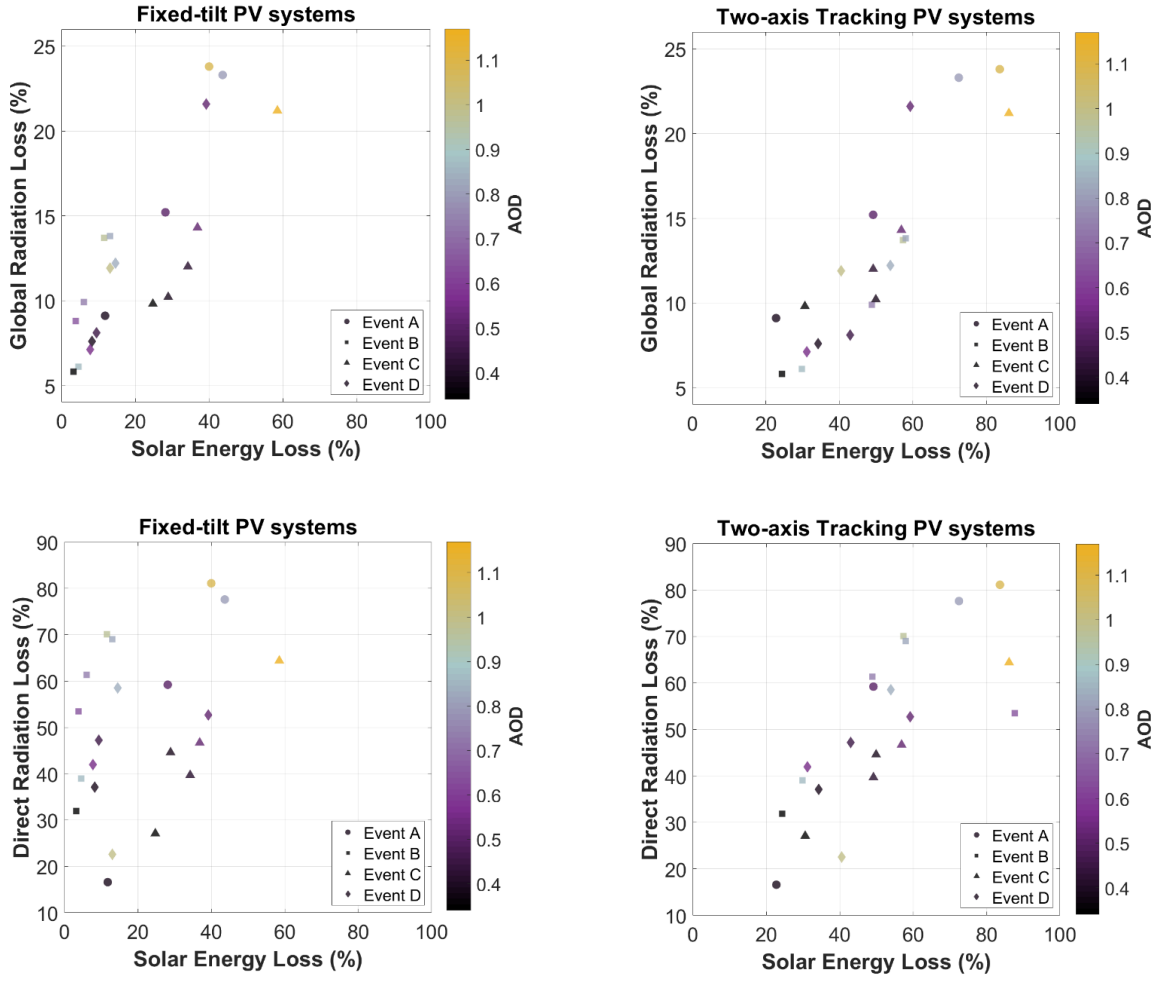

Figure 4: Global (top panel) and direct (lower panel) radiation losses (%) versus losses in produced solar energy (in %) during the four dust events for fixed-tilt PV systems (left) and two-axis tracking systems (right), along with AOD.

3.2 Effects of aerosol optical properties under variable conditions

In addition to the analysis described in Section 3.1 based on real atmospheric conditions during the four dust events in the Mediterranean Basin, a sensitivity analysis was performed to quantify how aerosol optical properties and solar geometry jointly influence PV energy production. The simulations considered representative aerosol conditions of Mediterranean dust intrusions, as described in Section 2.5 and Table 2, and evaluated their radiative impact across a wide range of SZAs. Unless otherwise stated, for the analysis, we assumed a south-oriented PV system (azimuth 180°), which corresponds to the typical optimal configuration for fixed PV installations in the Northern Hemisphere.

https://doi.org/10.5194/egusphere-2026-2775
Preprint. Discussion started: 27 May 2026

The sensitivity analysis was structured to isolate the influence of key atmospheric and geometrical parameters such as latitude, AOD, AE, and PV azimuth orientation. The resulting PV energy losses are expressed relative to aerosol-free atmospheric conditions and summarized in this section.

Across all scenarios, SZA emerges as the dominant driver of the observed PV energy losses. As shown in the figures of this section and in the Supplement (Fig. S1-4-7), aerosol-induced attenuation remained relatively small under high solar elevation conditions (SZA lower than approximately 30–35°), in most cases leading to losses that do not exceed 10–15%. However, SZA increases toward early morning, late afternoon, or wintertime conditions, leading to substantial atmospheric optical path length increases, resulting in progressively stronger attenuation of solar radiation and, therefore, energy output. Consequently, PV energy losses increased rapidly with increasing SZA, particularly under enhanced aerosol loading.

The latitude sensitivity analysis (Fig. S1), conducted for 25°, 35°, and 45° N under identical aerosol conditions, revealed only minor differences in the resulting PV energy losses when expressed as a function of SZA. In order to further quantify the relative importance of each parameter, additional difference maps were computed, representing the incremental change in PV energy losses between selected parameter ranges while keeping all other variables fixed. This indicates that, for a given SZA, aerosol-induced radiative attenuation is primarily governed by solar geometry and relatively independent of geographic latitude. Although in general higher latitudes experience larger SZAs on average throughout the year, the modest variations in solar incidence angles on the plane of the PV panels across the examined, relatively narrow latitudinal range, representative of the Mediterranean region, lead to nearly identical instantaneous PV energy losses, as they are primarily governed by the incident solar geometry. The corresponding difference analysis confirms that inter-latitudinal variations remain small, typically not exceeding 5–6% across the examined conditions Figure 4. However, some differences due to latitude may, in real atmospheric conditions, also derive from other parameters, such as water vapor and temperature, which are not accounted for in the present sensitivity analysis.

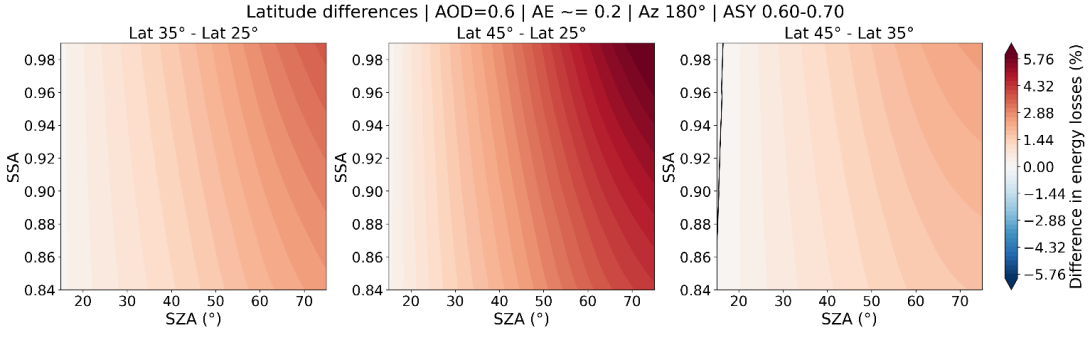

Figure 5: Differences in PV energy losses (%) as a function of solar zenith angle (SZA) and single-scattering albedo (SSA) for the latitude sensitivity analysis, under fixed aerosol optical depth (AOD = 0.6), Ångström exponent (AE ≈ 0.2), south-facing orientation (Az = 180°), and asymmetry parameter range ASY = 0.60–0.70.

In contrast, the AOD sensitivity analysis clearly demonstrates the strong amplification of PV energy losses with increasing aerosol concentration (Fig. S2). Based on the findings of the latitudinal sensitivity and the negligible differences across the different cases, a representative latitude of 35° N was adopted for all subsequent sensitivity analysis. For relatively moderate

https://doi.org/10.5194/egusphere-2026-2775
Preprint. Discussion started: 27 May 2026

aerosol levels (AOD = 0.2), losses remain limited at low and moderate SZAs but increase significantly beyond approximately 55°–60°. Under elevated dust concentrations (AOD = 0.6), strong attenuation develops already at intermediate SZAs (45–50°), while losses exceeding 60–70% occur at the highest SZAs considered. For extreme aerosol loading (AOD = 1.0), PV losses become substantial across nearly the entire SZA range. This behaviour is further quantified by the difference analysis in Figure 5, which shows that increasing AOD from 0.2 to 1.0 results in additional PV energy losses exceeding 40% at large SZAs. Even moderate increases (e.g., AOD 0.6 relative to 0.2) lead to differences on the order of 20–30%, particularly beyond SZA ≈ 50°.

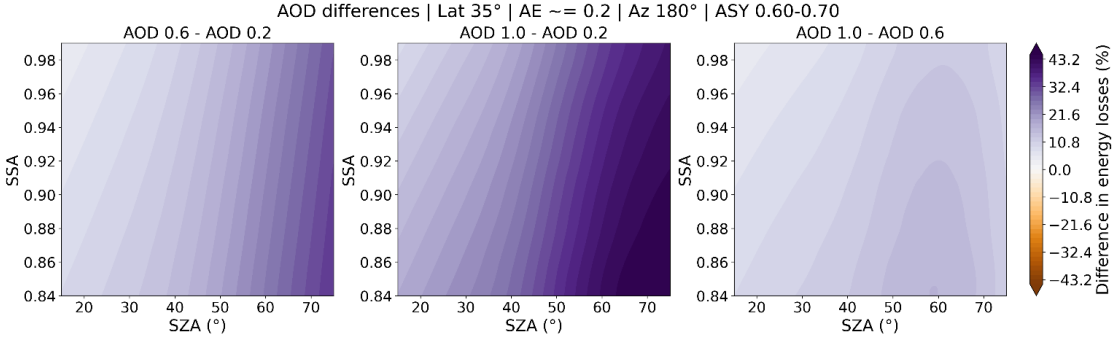

Figure 6: Differences in PV energy losses (%) as a function of solar zenith angle (SZA) and single-scattering albedo (SSA) for the AOD sensitivity analysis, under fixed latitude (35°), Ångström exponent (AE ≈ 0.2), south-facing orientation (Az = 180°), and asymmetry parameter range ASY = 0.60–0.70. Panels show the pairwise differences in losses between AOD values of 0.6 and 0.2, 1.0 and 0.2, and 1.0 and 0.6.

Investigation of the AE impact (Fig. S3) provides insight into the role of aerosol particle size distribution, comparing coarse-mode dominated dust conditions (AE = 0.0–0.2) with slightly more mixed aerosol regimes (AE = 0.2–0.4). The results indicate relatively modest differences between the two regimes, with the coarse-mode dominated cases generally producing slightly higher PV energy losses, particularly at large SZAs. The difference analysis in Figure 6 indicates that variations in AE result in changes in PV energy losses generally below 3–4%, with slightly higher losses associated with coarse-mode particles at large SZAs.

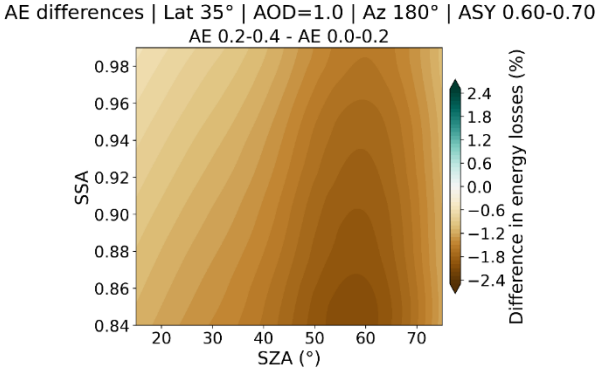

Figure 7: Differences in PV energy losses (%) as a function of solar zenith angle (SZA) and single-scattering albedo (SSA) for the Ångström exponent sensitivity analysis, under fixed latitude (35°), aerosol optical depth (AOD = 1.0), south-facing orientation (Az = 180°), and asymmetry parameter range ASY = 0.60–0.70. The panel shows the difference in losses between the AE intervals 0.2–0.4 and 0.0–0.2.

https://doi.org/10.5194/egusphere-2026-2775
Preprint. Discussion started: 27 May 2026

Finally, regarding the PV orientation sensitivity analysis (Fig. S4), we compared east-facing (90°), southeast-facing (130°), and south-facing (180°) configurations. The results indicate moderate variations in PV energy losses among the different orientations, with the south-facing configuration generally experiencing slightly larger aerosol-induced losses at high SZAs arising from its stronger alignment with the solar trajectory during peak irradiance periods. The difference analysis (Fig 7) shows that orientation effects can reach up to approximately 30% at high SZAs when comparing east- and south-facing configurations.

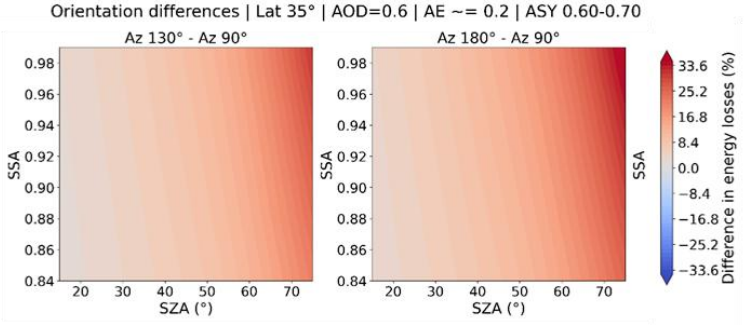

Figure 8: Differences in PV energy losses (%) as a function of solar zenith angle (SZA) and single-scattering albedo (SSA) for the panel-orientation sensitivity analysis, under fixed latitude (35°), aerosol optical depth (AOD = 0.6), Ångström exponent (AE ≈ 0.2), and asymmetry parameter range ASY = 0.60–0.70.

3.3 Estimation of PV output using ground-based measurements and METAL-WRF

In this section, we compare the PV output that has been estimated from the modelled irradiances with the PV output that has been estimated from ground-based measurements, indicatively for two stations that have been affected by dust from the Sahara (Lampedusa, during event D) and the Middle East (Agia Marina Xyliatou- AMX, during event C). In particular, we compare modelled PV outputs when GSEE inputs are irradiances that have been measured at the surface level, and irradiances from libRadtran (retrieved as described in Sect. 2.3) and the METAL-WRF model.

In previous works (Spyrou et al., 2025; Papetta et al., 2026), the efficiency of METAL-WRF in reproducing dust optical properties, as well as in simulating the GHI using its RT scheme, has been evaluated. In this work, we try to assess how accurately it can quantify solar power potential when it is coupled with a PV output model (GSEE), with respect to the reference case where GSEE inputs are ground-based measurements.

We compare the daily PV output for three different cases, when calculated based on ground-based measurements, METAL-WRF, and libRadtran, respectively (Fig.11). For the comparison, we used measurements of the global (GHI) and diffuse (DHI) surface solar irradiance from pyranometers operating at the two selected stations. For the selected period, data under all atmospheric conditions are presented, Cloudy and cloud-free days have been identified visually from the timeseries of the GHI (shown in Fig. 9). For instance, in the case of AMX, during days 2, 3, 5 and 7 clear-sky conditions dominated, while in the case of Lampedusa, days 1, 6, 7, 8 and 9 indicated cloudy conditions.

https://doi.org/10.5194/egusphere-2026-2775
Preprint. Discussion started: 27 May 2026

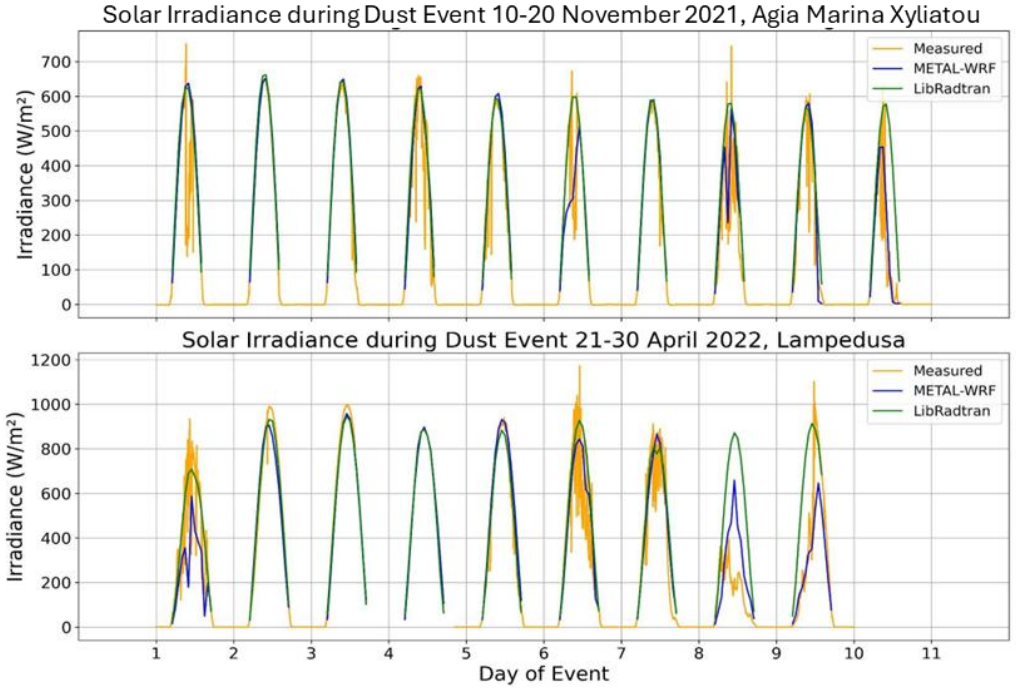

Figure 9: Timeseries of the GHI at Agia Marina Xyliatou, Cyprus, during event C (upper panel) and Lampedusa, Italy, during Event D (lower panel).

The evolution of the AOD at 500 nm from AERONET and the DOD at 500 nm from METAL-WRF is shown in Fig.10 . In the case of AMX, METAL-WRF underestimates AOD values, although it follows the evolution of the event. As discussed in Papetta et al. (2026), this is possibly due to anthropogenic particles that are included in the mixture and not considered by METAL-WRF. In the case of Lampedusa, dust in the aerosol mixture is more dominant. DOD from METAL-WRF follows the AOD closely, although differences are occasionally large, especially when AOD is very high. This is associated with the uncertainties in the description of the timing and the magnitude of the events (Solomos et al., 2023).

https://doi.org/10.5194/egusphere-2026-2775
Preprint. Discussion started: 27 May 2026

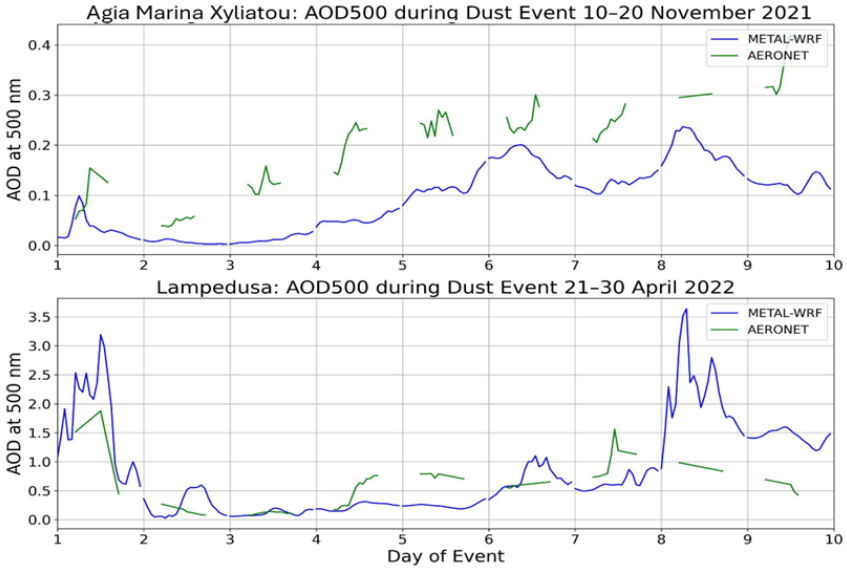

Figure 10: AOD at 500 nm from AERONET (green line) and METAL-WRF (blue line) for Agia Marina Xyliatou (upper panel) and Lampedusa (lower panel). The presented AERONET values are those interpolated to the time of the simulations as described in Sect. 2.3.

A comparison between the daily GHI from libRadtran and METAL-WRF for the days of the event is shown in Fig. 11. For the daily GHI values, the full dataset was used without cloudy conditions being filtered out, since METAL-WRF represents all atmospheric conditions. During cloudless sky days (with respect to the ones indicated as clear-sky based on Fig.9), the comparison between modelled and measured GHI revealed an agreement in most cases better than 10%. The overestimation of GHI in cloudy days lies in the fact that libRadtran simulations were performed for clear-sky conditions, neglecting the effect of clouds.

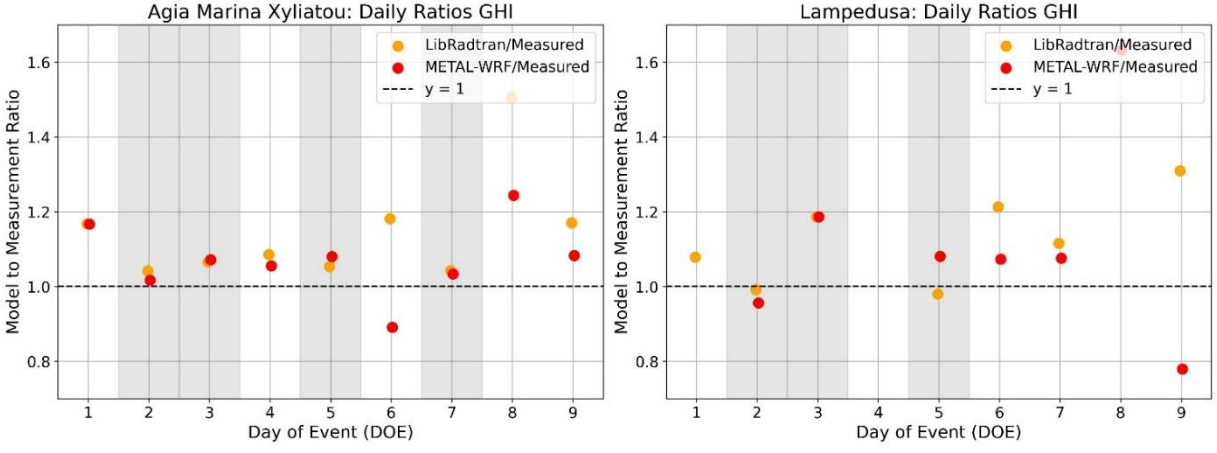

Figure 11: Ratios of GHI from libRadtran (orange) and METAL-WRF (red) to measured GHI at Agia Marina Xyliatou (left) and Lampedusa (right).

https://doi.org/10.5194/egusphere-2026-2775
Preprint. Discussion started: 27 May 2026

To further investigate the behaviour of the different irradiance components, such as GHI and DNI from libRadtran and METAL-WRF, we focused on two mostly clear-sky days, one for AMX and one for Lampedusa station. For each case study, we present the ratio between modelled (from libRadtran and METAL-WRF) and measured values of the afore-mentioned components during the selected days (Fig.12). More precisely, for AMX, the second day of the event is presented, while for Lampedusa, the fifth day was selected (as indicated in Fig.11), corresponding to 11/11/2021 and 25/04/2022, respectively. In terms of aerosols, in the case of Lampedusa, the load was significantly more enhanced than in the case of AMX, reaching approximately 0.8 compared to 0.07 based on AERONET retrievals (Fig.10). Based on complementary ground-based observations (Fig. S5 and Fig. S6), an aerosol layer was detected up to 4 km altitude in the case of Lampedusa, whereas in the case of AMX, it did not exceed 2 km. The timeseries of the ratios during the selected cases revealed an overall quite good agreement between modelled and measured parameters, with larger differences being observed for higher SZA's, specifically in the case of AMX, while a threshold of SZA<85° was applied in the comparisons of both cases.

For AMX, the comparison with libRadtran revealed a very good agreement, slightly overestimating the GHI throughout the entire day, while the METAL-WRF model revealed larger deviations for larger SZAs. However, this is not reflected in the daily ratios illustrated in Fig.11. For Lampedusa, the behaviour of the two models was reversed, with the METAL-WRF to measured ratio very close to unity overall, but larger deviations in the morning and the afternoon, when collocated ground-based Ceilometer observations revealed the presence of clouds (see Fig. S6).

In both stations, the DNI component revealed higher deviations than GHI. Considering that the direct component is primarily affected by AOD and the diffuse component is also influenced by other aerosol optical properties, the respective ratios denote that these parameters may not be fully represented in the simulations. Moreover, these effects are more pronounced for higher AOD values, which explains the more pronounced deviations in the case of Lampedusa. For lower aerosol load conditions, additional cases were analysed, which confirmed the findings illustrated for AMX, however, these results are not presented in this study.

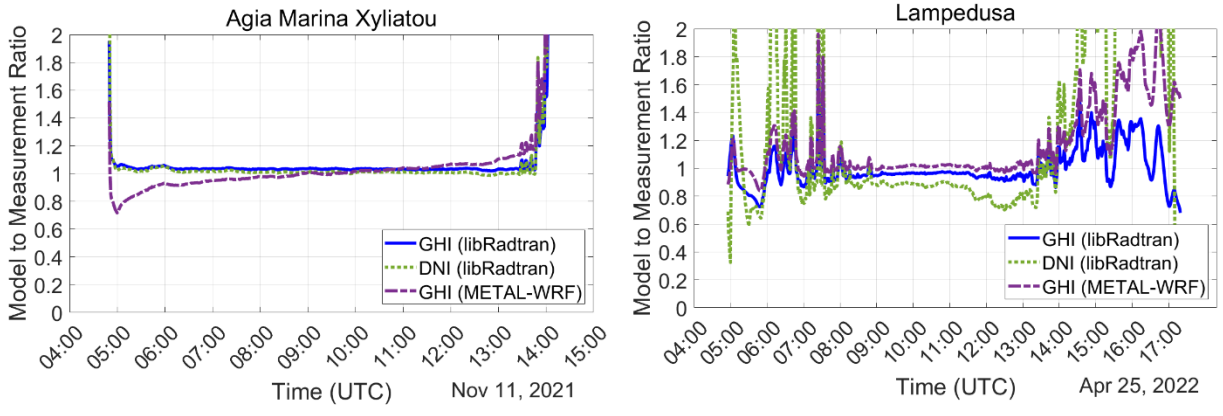

Figure 12: Ratios of modelled (libRadtran and METAL-WRF) to measured irradiances for a selected day at Agia Marina Xyliatou (left) and Lampedusa (right). GHI and DNI as calculated from the libRadtran model have been compared with the respective measured components, while only the comparison of GHI is presented in the case of METAL-WRF.

https://doi.org/10.5194/egusphere-2026-2775
Preprint. Discussion started: 27 May 2026

The ratio between the PV output from METAL-WRF (PV_{wrf}) and measurements, as well as the ratio between PV output from libRadtran (PV_{lbr}) and measurements, is presented in Fig. 13. PV output from libRadtran and from METAL-WRF has been simulated using only GHI as input to GSEE. The PV output from ground-based measurements has been retrieved using either only GHI (PV_{ghi}), or both GHI and DHI (PV_{ghi_dhi}). In addition, all the comparisons have been conducted for two PV orientations (optimally inclined: axis=0 and installed on a solar tracker that follows the sun: axis=2).

Comparing PV_{wrf} and PV_{lbr} with PV_{ghi} provides an estimate of how the differences between the modelled and the measured GHI impact the modelled PV output. Comparing PV_{wrf} and PV_{lbr} with PV_{ghi_dhi} results in generally larger deviations from unity (with respect to the ratios with PV_{ghi}), which are due to the fact that only the GHI has been used to simulate PV_{wrf} and PV_{lbr}, i.e., uncertainties in the parameterization of the diffuse component in GSEE when DHI is not available (Papadimitriou et al., 2026).

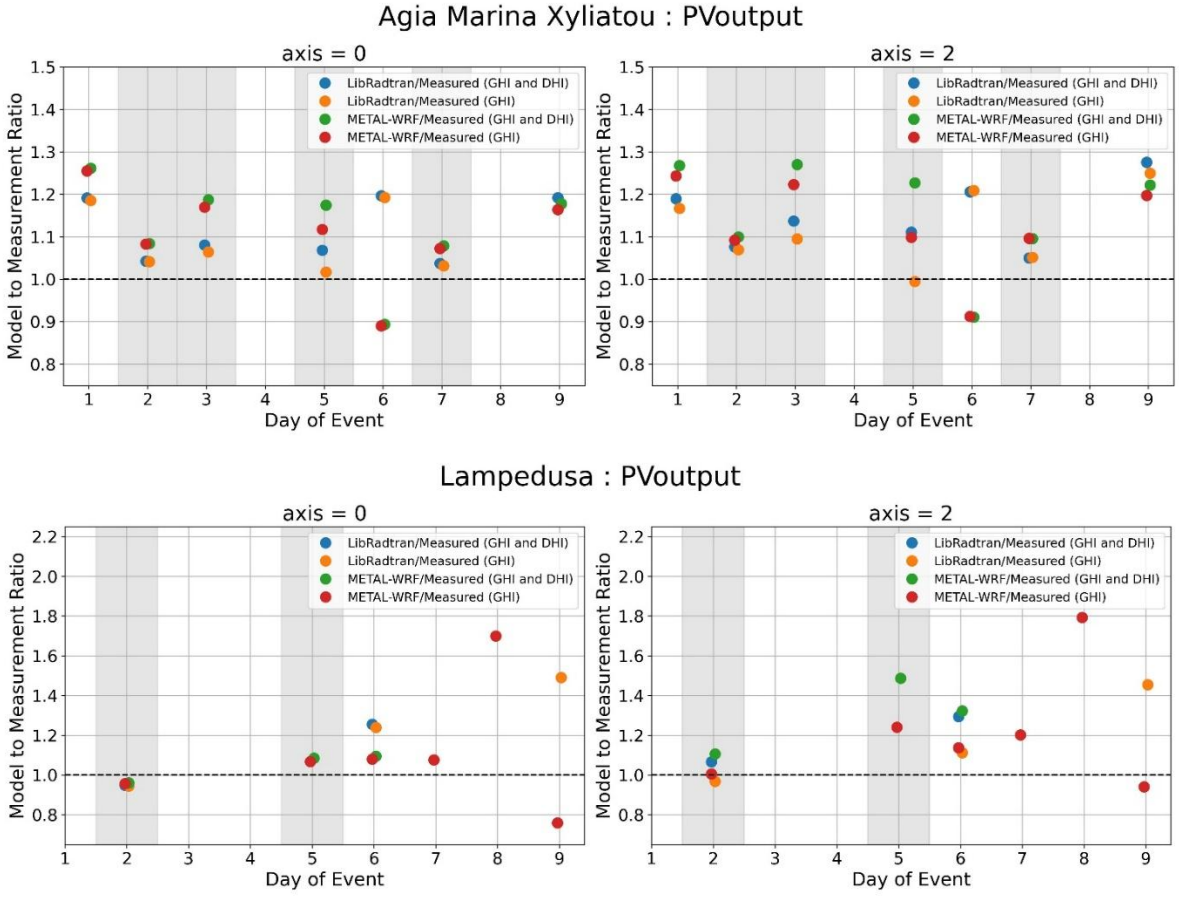

Figure 13: Ratios between PV_{lbr} and PV_{wrf} for Agia Marina Xyliatou (upper panels) and Lampedusa (lower panels), and for two panel setups: optimally inclined PVs (left panels), and 2-dimensional solar tracking PVs (right panels).

Although GHI values and model to measurement ratios of GHI have previously been presented for the entire period of the selected dust events for both AMX and Lampedusa (Fig. 9 and 11), in the case of Lampedusa some of the days are not presented

https://doi.org/10.5194/egusphere-2026-2775
Preprint. Discussion started: 27 May 2026

in Fig. 13. These days have been excluded to avoid biases into the analysis due to missing DHI (or GHI and DHI) measurements that did not allow the calculation of the daily integrals. As already discussed in Sect. 2.3 PV_{lbr} has been retrieved with the assumption of cloudless skies, even during cloudy days, which strongly impacts the ratios in specific cases. For example, clouds have impacted GHI over AMX in days 6 and 9, which is depicted in the larger, relatively on other days, differences between PV_{lbr} and PV_{ghi}/ PV_{ghi_dhi}. This also applies to days 6 - 9 at Lampedusa.

In (mostly) cloudless days, for static PVs (axis=0), the ratios between PV_{lbr} (or PV_{wrf}) and PV_{ghi} are very similar to the ratios between PV_{lbr} (or PV_{wrf}) and $PV_{ghi\_dhi,}$ showing that even under intense dust events, not including the DHI component in GSEE simulations is not critical for static, optimally inclined PVs. Differences become slightly more significant for the solar tracking PVs, generally not exceeding 10%.

Comparing PV_{wrf} (that takes cloudiness into account) with PV_{ghi} and PV_{ghi_dhi} shows that including the DHI component in the simulations is more significant for cloudy days. In these days, including or not including the DHI in the simulation results in large differences. For example, on day 9 for Lampedusa, the ratios between PV_{wrf} and PV_{ghi_dhi} exceed 2.5 and are out of the range of the graph.

Over AMX (event C), the dust plume is mixed with fine aerosols, as also discussed in Papetta et al. (2026). The fine aerosol component is not captured by METAL-WRF, which generally results in overestimation of the GHI, and subsequently an average overestimation in the daily PV output of the order of 10% (for both fixed PVs and PVs on solar tracking systems) during cloudless days. Over Lampedusa (event D), the aerosol mixture is constituted mainly by dust (see also Papetta et al., 2026), and the event is much stronger relative to the event over AMX. However, the cloudless sky days are very few to estimate the impact of this variability. In addition, the observed relative differences of AOD at 500 nm from AERONET and METAL-WRF (presented earlier in Fig.10) are reflected in the ratios of Fig.13 for the clear-sky conditions. More precisely, for AMX, the difference of the AOD retrievals is more pronounced during the fifth day compared to the second day, which can also explain the lower model-to-measurement ratio differences between the two models during the latter. The same was observed in the case of Lampedusa.

METAL-WRF captures the effect of cloudiness on daily GHI generally well for the most cloudy days of the two events. On day 8 of the event C, METAL-WRF, despite the fact that it identifies the presence of clouds, it overestimates (the very low) GHI significantly, by more than 50%, which results in an overestimation of ~ 70% for static PVs, and an overestimation of ~ 80% for solar tracking PVs. Comparison between PV_{wrf} and PV_{ghi} at Lampedusa during cloudy days yields similar results to the results for AMX. Nevertheless, the differences between PV_{wrf} and PV_{ghi_dhi} are significantly larger occasionally. The agreement between PV_{lbr} and PV_{ghi} (or PV_{ghi_dhi}) is worse than the agreement between PV_{wrf} and PV_{ghi} (or PV_{ghi_dhi}) on cloudy days, as expected, since clouds have not been considered in libRdtran simulations. It is interesting, however, that the agreement between PV_{wrf} and PV_{ghi} is similar to the agreement between PV_{lbr} and PVghi, even under cloudless skies.

https://doi.org/10.5194/egusphere-2026-2775
Preprint. Discussion started: 27 May 2026

4 Summary and conclusions

Global and direct solar irradiance measurements and respective simulations using aerosol properties observations can be of great value for solar energy production estimation. Our study focuses on the evaluation of the impact of atmospheric dust during four severe dust events on solar radiation and PV energy production potential over the Mediterranean Basin for the period 2021-2022. During dust events, the reduction is mainly correlated with AOD, regarding the aerosol parameters, and different PV installation structures, e.g., fixed-tilt and two-axis tracking systems. The radiative effects on the different components of solar radiation, such as DNI and GHI, can be affected differently, which is also reflected in the PV energy production potential of each tracking system as well.

We investigated the impact of dust on the levels of the SSR, which, overall, revealed a systematically more significant dust-induced attenuation in DNI, with maximum losses frequently exceeding 60–80%, while GHI attenuation typically ranged between 5% and 25%. Further assessment of these findings on PV system performance and solar energy production showed that substantial PV power output losses for both fixed-tilt and two-axis tracking systems reached ~45% and 80%, respectively, with the impact on the latter being significantly higher, highlighting the pronounced sensitivity of the tracking systems to DNI. The afore-mentioned results indicate that, although tracking systems generally outperform fixed installations under clear-sky conditions, their relative vulnerability to intense dust episodes becomes evident during high dust-load conditions and, therefore, their efficiency experiences more fluctuations in areas that experience such events.

A sensitivity test on AOD, SSA, and AE as a function of different SZAs, latitudes, and azimuth orientation showed that SZA emerges as the major factor controlling PV energy losses, followed by AOD, causing substantial losses regardless of the SZA under severe aerosol loads (AOD=1.0). The role of aerosol particle size distribution was found to be less significant, however, coarse-mode dominated events generally lead to slightly altered PV energy losses. Latitude and orientation variability played a minor role overall, with south-facing configuration experiencing more pronounced aerosol-induced losses at high SZAs due to its stronger alignment with the solar trajectory under peak solar radiation conditions.

Further investigation into two extended events at Agia Marina Xyliatou in Cyprus and Lampedusa in Italy revealed quite good agreement among AERONET and METAL-WRF AOD retrievals, with some exceptions. For cloudless conditions, when aerosols are the main attenuator of solar radiation and energy, a comparison between modelled GHI from two RT models (libRadtran with inputs from AERONET and METAL-WRF) with ground-based solar radiation observations leads to differences smaller than 10% in the case of AERONET, while the implementation of the METAL-WRF model leads to differences of up to 20%. Using both diffuse and global solar irradiance aspects in GSEE seems to provide better results.

Under cloudy conditions, the comparisons lead to greater differences and an overall overestimation in the case of libRadtran, which was performed for cloudless sky conditions. Furthermore, using the DHI component in GSEE simulations is not a critical parameter for fixed, optimally inclined PVs under cloudless sky conditions, in contrast to cloudy sky conditions, when it is particularly important. Under these conditions, neglecting DHI can lead to large discrepancies in PV estimates, with ratios in some cases exceeding 2.5.

https://doi.org/10.5194/egusphere-2026-2775
Preprint. Discussion started: 27 May 2026

Overall, our analysis denotes that the estimated impact of dust on energy potential is very large, well beyond the uncertainty levels in our simulations, while differences to simulated PV output when ground-based measurements were used as inputs are mostly related to uncertainties in the parameterization of aerosols and clouds.

This study focused on the dust direct radiative effects, however, additional processes that are not taken into account in this study, such as soiling on PV systems, the indirect effect of dust through cloud formation, may further affect PV energy production and should be further investigated.

Author contributions

Conceptualization, D.K., G.C. and I.F.; methodology, D.K., G.C. and I.F.; software, D.K., G.C. and N.P.; validation, S.K.; formal analysis, D.K., G.C. and I.F.; investigation, D.K., G.C., A.M., A.P., C.H.-A., Y.A., S.H.-A., M.M., N.P. and I.F.; data curation, D.K., G.C., A.P., C.H.-A. and N.P.; Visualization, D.K., G.C., R.-T.C. and K.A; writing, original draft preparation, D.K., G.C.; writing, review and editing, all authors; supervision, I.F., S.S. and S.K.; project administration, S.K.; Resources, C.S., D.M., K.F., Y.D., T.I., R.-E. M. and S.S.; funding acquisition, S.K. All authors have read and agreed to the published version of the manuscript.

Competing interests

At least one of the (co-)authors is a member of the editorial board of Atmospheric Measurement Techniques.

Acknowledgements

This study is based on the work from COST Action HARMONIA (CA21119), supported by COST (European Cooperation in Science and Technology). DK would like to acknowledge the Obs3RvE (Optimising 3D RT Earthcare product using geostationary observations and AI) project, funded from the European Space Agency under Contract No. 4000147848/25/I/AG, and the AIRSENSE (Aerosol and aerosol cloud Interaction from Remote SENSing Enhancement) project, funded from the European Space Agency under Contract No. 4000142902/23/I-NS. GC would like to acknowledge the EXCELSIOR: ERATOSTHENES: Excellence Research Centre for Earth Surveillance and Space-Based Monitoring of the Environment H2020 Widespread Teaming project (www.excelsior2020.eu, accessed on 13 March 2023). The EXCELSIOR project has received funding from the European Union's Horizon 2020 Research and Innovation Programme under Grant Agreement No 857510, from the Government of the Republic of Cyprus through the Directorate General for the European Programmes, Coordination and Development and the Cyprus University of Technology and ATARRI: This project has received funding from the European Union's Horizon Europe Twinning Call (HORIZON-WIDERA-2023-ACCESS-02) under the grant agreement No 101160258. AP and KF acknowledge EMMECARE and DUST-DN projects for supporting this work

https://doi.org/10.5194/egusphere-2026-2775
Preprint. Discussion started: 27 May 2026

under the European Union's Horizon 2020 Research and Innovation Programme (Grant Agreement No. 856612 and 101168425). SK would like to acknowledge the Solid PV project (24GRD04 SOLiD-PV) funded from the European Partnership on Metrology, co-financed from the European Union's Horizon Europe Research and Innovation Programme and by the Participating States.

This research was supported by ENEA within the framework of the Electric System Research Programme (Three-Year Implementation Plan 2025–2027), Project 1.5 "High efficiency buildings for the energy transition", Work Package 2: "Models, strategies and technological solutions for energy efficiency at the service of the territory", financed by the Ministry for the Environment and Energy Security. CUP: I53C24003330001. Contributions by Damiano Sferlazzo at Lampedusa are gratefully acknowledged. The support of ACTRIS-ERIC and the University of Valladolid concerning the AERONET photometer calibration at Lampedusa is gratefully acknowledged. The authors would also like to thank the PIs of the AERONET network stations considered in the present study.

Financial support COST Action HARMONIA (CA21119), supported by COST (European Cooperation in Science and Technology)

References

Abadi, A. R. S., Hamzeh, N. H., Kaskaoutis, D. G., Xu, B., Li, L., & Ghassabi, Z.: Future Projections of Dust Storm Dynamics and Sources in the Middle East: Insights from CMIP6 Models. Atmospheric Pollution Research, 102775, 2025.

Adebiyi, A. A., et al.: A review of coarse mineral dust in the Earth system, Preprint at EarthArXiv, https://doi.org/10.31223/X5QD36, 2022.

Alonso-Montesinos, J., Martínez, F. R., Polo, J., Martín-Chivelet, N., and Batlles, F. J.: Economic effect of dust particles on photovoltaic plant production, Energies, 13(23), 6376, https://doi.org/10.3390/en13236376, 2020.

Amiridis, V., Marinou, E., Tsekeri, A., Wandinger, U., Schwarz, A., Giannakaki, E., Mamouri, R., Kokkalis, P., Binietoglou, I., Solomos, S., Herekakis, T., Kazadzis, S., Gerasopoulos, E., Proestakis, E., Kottas, M., Balis, D., Papayannis, A., Kontoes, C., Kourtidis, K., Papagiannopoulos, N., Mona, L., Pappalardo, G., Le Rille, O., and Ansmann, A.: LIVAS: a 3-D multi-wavelength aerosol/cloud database based on CALIPSO and EARLINET, Atmos. Chem. Phys., 15, 7127–7153, https://doi.org/10.5194/acp-15-7127-2015, 2015.

Anderson, G., Clough, S., Kneizys, F., Chetwynd, J., and Shettle, E.: AFGL atmospheric constituent profiles (0–120 km), Tech. Rep. AFGL-TR-86-0110, Air Force Geophys. Lab., Hanscom Air Force Base, Bedford, Mass., 1986.

Antón, M., Valenzuela, A., Cazorla, A., Gil, J. E., Fernández-Gálvez, J., Lyamani, H., ... & Alados-Arboledas, L.: Global and diffuse shortwave irradiance during a strong desert dust episode at Granada (Spain). Atmospheric research, 118, 232-239.https://doi.org/10.1016/j.atmosres.2012.07.007, 2012.

https://doi.org/10.5194/egusphere-2026-2775
Preprint. Discussion started: 27 May 2026

Aslanoğlu, S. Y., Proestakis, E., Gkikas, A., Güllü, G., Amiridis, V.: Dust Climatology of Turkey as a Part of the Eastern Mediterranean Basin via 9-Year CALIPSO-Derived Product, Atmosphere, 13(5), 733, https://doi.org/10.3390/atmos13050733, 2022.

Boucher, O.: Aerosol–Cloud Interactions. In Atmospheric Aerosols: Properties and Climate Impacts (pp. 193-226). Dordrecht: Springer Netherlands, 2015.

Buehler, S. A., John, V. O., Kottayil, A., Milz, M., and Eriksson, P.: Efficient radiative transfer simulations for a broadband infrared radiometer - combining a weighted mean of representative frequencies approach with frequency selection by simulated annealing, J. Quant. Spectrosc. Radiat. Transfer, 111, 602–615, 2010.

Buras, R., Dowling, T., and Emde, C.: New secondary-scattering correction in DISORT with increased efficiency for forward scattering, J. Quant. Spectrosc. Radiat. Transf., 112, 2028–2034, https://doi.org/10.1016/j.jqsrt.2011.02.023, 2011.

Callewaert, S., Vandenbussche, S., Kumps, N., Kylling, A., Shang, X., Komppula, M., Goloub, P., and De Mazière, M.: The Mineral Aerosol Profiling from Infrared Radiances (MAPIR) algorithm: version 4.1 description and evaluation, Atmos. Meas. Tech., 12, 3673–3698, https://doi.org/10.5194/amt-12-3673-2019, 2019.

Che, H., Qi, B., Zhao, H., Xia, X., Eck, T. F., Goloub, P., Dubovik, O., Estelles, V., Cuevas-Agulló, E., Blarel, L., Wu, Y., Zhu, J., Du, R., Wang, Y., Wang, H., Gui, K., Yu, J., Zheng, Y., Sun, T., Chen, Q., Shi, G., and Zhang, X.: Aerosol optical properties and direct radiative forcing based on measurements from the China Aerosol Remote Sensing Network (CARSNET) in eastern China, Atmos. Chem. Phys., 18, 405–425, https://doi.org/10.5194/acp-18-405-2018, 2018.

Cuevas-Agulló, E., Barriopedro, D., García, R. D., Alonso-Pérez, S., González-Alemán, J. J., Werner, E., Suárez, D., Bustos, J. J., García-Castrillo, G., García, O., Barreto, Á., and Basart, S.: Sharp increase in Saharan dust intrusions over the western Euro-Mediterranean in February–March 2020–2022 and associated atmospheric circulation, Atmos. Chem. Phys., 24, 4083–4104, https://doi.org/10.5194/acp-24-4083-2024, 2024.

Denjean, C., et al.: Size distribution and optical properties of African mineral dust after intercontinental transport, J. Geophys. Res. Atmos., 121, 7117–7138, https://doi.org/10.1002/2016JD025115, 2016.

Di Biagio, C., Balkanski, Y., Albani, S., Boucher, O., & Formenti, P.: Direct radiative effect by mineral dust aerosols constrained by new microphysical and spectral optical data. Geophysical Research Letters, 47, e2019GL086186. https://doi.org/10.1029/2019GL086186, 2020.

Drugé, T., Nabat, P., Mallet, M., and Somot, S.: Model simulation of ammonium and nitrate aerosols distribution in the Euro-Mediterranean region and their radiative and climatic effects over 1979–2016, Atmos. Chem. Phys., 19, 3707–3731, https://doi.org/10.5194/acp-19-3707-2019, 2019.

Dubovik, O., and M. D. King: A flexible inversion algorithm for retrieval of aerosol optical properties from Sun and sky radiance measurements, J. Geophys. Res., 105(D16), 20673–20696, doi:10.1029/2000JD900282, 2000.

Emde, C., et al.: The libRadtran software package for radiative transfer calculations (version 2.0.1), Geoscientific Model Development, 9(5), 1647–1672, 2016.

https://doi.org/10.5194/egusphere-2026-2775
Preprint. Discussion started: 27 May 2026

Engeland, K., Borga, M., Creutin, J.-D., François, B., Ramos, M.-H., and Vidal, J.-P.: Space-time variability of climate variables and intermittent renewable electricity production – A review, Renew. Sust. Energy Rev., 79, 600–617, https://doi.org/10.1016/j.rser.2017.05.046, 2017.

Engelstaedter, S., Tegen, I., and Washington, R.: North African dust emissions and transport, Earth-Sci. Rev., 79, 73–100, https://doi.org/10.1016/j.earscirev.2006.06.004, 2006.

Flaounas, E., Kotroni, V., Lagouvardos, K., Kazadzis, S., Gkikas, A., and Hatzianastassiou, N.: Cyclone contribution to dust transport over the Mediterranean region, Atmos. Sci. Lett., 16, 473–478, https://doi.org/10.1002/asl2.577, 2015.

Forkel, R., Werhahn, J., Hansen, A. B., McKeen, S., Peckham, S., Grell, G., & Suppan, P.: Effect of aerosol-radiation feedback on regional air quality–A case study with WRF/Chem. Atmospheric Environment, 53, 202-211, 2012.

Fountoulakis, I., Kosmopoulos, P., Papachristopoulou, K., Raptis, I.-P., Mamouri, R.-E., Nisantzi, A., Gkikas, A., Witthuhn, J., Bley, S., Moustaka, A., Buehl, J., Seifert, P., Hadjimitsis, D. G., Kontoes, C., & Kazadzis, S.: Effects of Aerosols and Clouds on the Levels of Surface Solar Radiation and Solar Energy in Cyprus. Remote Sensing, 13(12), 2319. https://doi.org/10.3390/rs13122319, 2021.

Fountoulakis, I., Natsis, A., Siomos, N., Drosoglou, T., & Bais, A. F.: Deriving Aerosol Absorption Properties from Solar Ultraviolet Radiation Spectral Measurements at Thessaloniki, Greece. Remote Sensing, 11(18), 2179. https://doi.org/10.3390/rs11182179, 2019.

Fountoulakis, I., Papachristopoulou, K., Proestakis, E., Amiridis, V., Kontoes, C., & Kazadzis, S.: Effect of Aerosol Vertical Distribution on the Modeling of Solar Radiation. Remote Sensing, 14(5), 1143. https://doi.org/10.3390/rs14051143, 2022.

Fountoulakis, I., Tsekeri, A., Kazadzis, S., Amiridis, V., Nersesian, A., Tsichla, M., Proestakis, E., Gkikas, A., Papachristopoulou, K., Barlakas, V., Emde, C., and Mayer, B.: A sensitivity study on radiative effects due to the parameterization of dust optical properties in models, Atmos. Chem. Phys., 24, 4915–4948, https://doi.org/10.5194/acp-24-4915-2024, 2024.

Francis, D., Fonseca, R., Nelli, N., Cuesta, J., Weston, M., Evan, A., & Temimi, M.: The atmospheric drivers of the major Saharan dust storm in June 2020. Geophysical Research Letters, 47(24), e2020GL090102, 2020.

Gasteiger, J., Emde, C., Mayer, B., Buras, R., Buehler, S., and Lemke, O.: Representative wavelengths absorption parameterization applied to satellite channels and spectral bands, J. Quant. Spectrosc. Radiat. Transfer, 148, 99–115, doi:10.1016/j.jqsrt.2014.06.024, 2014.

Giles, D. M., Sinyuk, A., Sorokin, M. G., Schafer, J. S., Smirnov, A., Slutsker, I., Eck, T. F., Holben, B. N., Lewis, J. R., Campbell, J. R., Welton, E. J., Korkin, S. V., and Lyapustin, A. I.: Advancements in the Aerosol Robotic Network (AERONET) Version 3 database – automated near-real-time quality control algorithm with improved cloud screening for Sun photometer aerosol optical depth (AOD) measurements, Atmos. Meas. Tech., 12, 169–209, https://doi.org/10.5194/amt-12-169-2019, 2019.

https://doi.org/10.5194/egusphere-2026-2775
Preprint. Discussion started: 27 May 2026

Gkikas, A., Basart, S., Hatzianastassiou, N., Marinou, E., Amiridis, V., Kazadzis, S., Pey, J., Querol, X., Jorba, O., Gassó, S., and Baldasano, J. M.: Mediterranean intense desert dust outbreaks and their vertical structure based on remote sensing data, Atmos. Chem. Phys., 16, 8609–8642, https://doi.org/10.5194/acp-16-8609-2016, 2016.

Gkikas, A., Hatzianastassiou, N., Mihalopoulos, N., Katsoulis, V., Kazadzis, S., Pey, J., Querol, X., and Torres, O.: The regime of intense desert dust episodes in the Mediterranean based on contemporary satellite observations and ground measurements, Atmos. Chem. Phys., 13, 12135–12154, https://doi.org/10.5194/acp-13-12135-2013, 2013.

Gkikas, A., Houssos, E. E., Lolis, C. J., Bartzokas, A., Mihalopoulos, N., and Hatzianastassiou, N.: Atmospheric circulation evolution related to desert-dust episodes over the Mediterranean, Q. J. R. Meteorol. Soc., 141, 1634–1645, https://doi.org/10.1002/qj.2466, 2015.

Gkikas, A., Obiso, V., Pérez García-Pando, C., Jorba, O., Hatzianastassiou, N., Vendrell, L., Basart, S., Solomos, S., Gassó, S., and Baldasano, J. M.: Direct radiative effects during intense Mediterranean desert dust outbreaks, Atmos. Chem. Phys., 18, 8757–8787, https://doi.org/10.5194/acp-18-8757-2018, 2018.

Gkikas, A., Proestakis, E., Amiridis, V., Kazadzis, S., Di Tomaso, E., Marinou, E., Hatzianastassiou, N., Kok, J. F., and García-Pando, C. P.: Quantification of the dust optical depth across spatiotemporal scales with the MIDAS global dataset (2003–2017), Atmos. Chem. Phys., 22, 3553–3578, https://doi.org/10.5194/acp-22-3553-2022, 2022.

Gkikas, A., Proestakis, E., Amiridis, V., Kazadzis, S., Di Tomaso, E., Tsekeri, A., Marinou, E., Hatzianastassiou, N., and Pérez García-Pando, C.: ModIs Dust AeroSol (MIDAS): a global fine-resolution dust optical depth data set, Atmos. Meas. Tech., 14, 309–334, https://doi.org/10.5194/amt-14-309-2021, 2021.

Go, S., Lyapustin, A., Schuster, G. L., Choi, M., Ginoux, P., Chin, M., Kalashnikova, O., Dubovik, O., Kim, J., da Silva, A., Holben, B., and Reid, J. S.: Inferring iron-oxide species content in atmospheric mineral dust from DSCOVR EPIC observations, Atmos. Chem. Phys., 22, 1395–1423, https://doi.org/10.5194/acp-22-1395-2022, 2022.

Gómez-Amo, J. L., Freile-Aranda, M. D., Camarasa, J., Estellés, V., Utrillas, M. P., and Martínez-Lozano, J. A.: Empirical estimates of the radiative impact of an unusually extreme dust and wildfire episode on the performance of a photovoltaic plant in the western Mediterranean, Appl. Energy, 235, 1226–1234, 2019.

Gómez-Amo, J. L., Pinti, V., Di Iorio, T., di Sarra, A., Meloni, D., Becagli, S., Bellantone, V., Cacciani, M., Fuà, D., and Perrone, M. R.: The June 2007 Saharan dust event in the central Mediterranean: Observations and radiative effects in marine, urban, and suburban environments, Atmos. Environ., 45, 5385–5493, 2011.

Haugvaldstad, O. W., Olivié, D., Storelvmo, T., and Schulz, M.: Dust radiative forcing in CMIP6 Earth System models: insights from the AerChemMIP piClim-2xdust experiment, Atmos. Chem. Phys., 25, 13199–13219, https://doi.org/10.5194/acp-25-13199-2025, 2025.

Haywood, J., and Boucher, O.: Estimates of the direct and indirect radiative forcing due to tropospheric aerosols: A review, Rev. Geophys., 38, 513–543, https://doi.org/10.1029/1999RG000078, 2000.

Holben, B. N., Eck, T. F., Slutsker, I. A., Tanre, D., Buis, J. P., Setzer, A., ... & Smirnov, A.: AERONET-A federated instrument network and data archive for aerosol characterization. Remote sensing of environment, 66(1), 1-16, 1998.

https://doi.org/10.5194/egusphere-2026-2775
Preprint. Discussion started: 27 May 2026

International Energy Agency (IEA): World Energy Outlook 2023: Executive Summary, retrieved from https://www.iea.org/reports/world-energy-outlook-2023/executive-summary, 2023.

International Renewable Energy Agency (IRENA): Renewable capacity statistics 2023, retrieved from https://www.irena.org/Statistics, 2023.

Jish Prakash, P., Stenchikov, G., Kalenderski, S., Osipov, S., and Bangalath, H.: The impact of dust storms on the Arabian Peninsula and the Red Sea, Atmos. Chem. Phys., 15, 199–222, doi:10.5194/acp-15-199-2015, 2015.

Kato, S., Ackerman, T. P., Mather, J. H., and Clothiaux, E.: The k-distribution method and correlated-k approximation for a shortwave radiative transfer model, J. Quant. Spectrosc. Radiat. Transfer, 62, 109–121, 1999.

Kazadzis, S., Founda, D., Psiloglou, B. E., Kambezidis, H., Mihalopoulos, N., Sanchez-Lorenzo, A., Meleti, C., Raptis, P. I., Pierros, F., and Nabat, P. (2018). Long-term series and trends in surface solar radiation in Athens, Greece, Atmos. Chem. Phys., 18, 2395–2411, https://doi.org/10.5194/acp-18-2395-2018.

Kazadzis, S., Raptis, P., Kouremeti, N., Amiridis, V., Arola, A., Gerasopoulos, E., and Schuster, G. L.: Aerosol absorption retrieval at ultraviolet wavelengths in a complex environment, Atmos. Meas. Tech., 9, 5997–6011, https://doi.org/10.5194/amt-9-5997-2016, 2016.

Kok, J. F., Adebiyi, A. A., Albani, S., Balkanski, Y., Checa-Garcia, R., Chin, M., Colarco, P. R., Hamilton, D. S., Huang, Y., Ito, A., Klose, M., Li, L., Mahowald, N. M., Miller, R. L., Obiso, V., Pérez García-Pando, C., Rocha-Lima, A., and Wan, J. S.: Contribution of the world's main dust source regions to the global cycle of desert dust, Atmos. Chem. Phys., 21, 8169–8193, https://doi.org/10.5194/acp-21-8169-2021, 2021.

Kok, J. F., Storelvmo, T., Karydis, V. A., Adebiyi, A. A., Mahowald, N. M., Evan, A. T., ... & Leung, D. M.: Mineral dust aerosol impacts on global climate and climate change. Nature Reviews Earth & Environment, 4(2), 71-86, 2023.

Kosmopoulos, P. G., Kazadzis, S., El-Askary, H., Taylor, M., Gkikas, A., Proestakis, E., Kontoes, C., & El-Khayat, M. M.: Earth-Observation-Based Estimation and Forecasting of Particulate Matter Impact on Solar Energy in Egypt. Remote Sensing, 10(12), 1870. https://doi.org/10.3390/rs10121870, 2018.

Kosmopoulos, P. G., Kazadzis, S., Taylor, M., Athanasopoulou, E., Speyer, O., Raptis, P. I., Marinou, E., Proestakis, E., Solomos, S., Gerasopoulos, E., Amiridis, V., Bais, A., and Kontoes, C.: Dust impact on surface solar irradiance assessed with model simulations, satellite observations and ground-based measurements, Atmos. Meas. Tech., 10, 2435–2453, https://doi.org/10.5194/amt-10-2435-2017, 2017.

Kouklaki, D., Kazadzis, S., Raptis, I.-P., Papachristopoulou, K., Fountoulakis, I., and Eleftheratos, K.: Photovoltaic spectral responsivity and efficiency under different aerosol conditions, Energies, 16(18), 6644, https://doi.org/10.3390/en16186644, 2023.

Kurucz, R.: Synthetic infrared spectra, in: Proceedings of the 154th Symposium of the International Astronomical Union (IAU); Tucson, Arizona, March 2-6, 1992, Kluwer, Acad., Norwell, MA, 1992.

Lauret, P., Boland, J., and Ridley, B.: Bayesian statistical analysis applied to solar radiation modelling, Renew. Energy, 49, 124–127, https://doi.org/10.1016/j.renene.2012.01.049, 2013.

https://doi.org/10.5194/egusphere-2026-2775
Preprint. Discussion started: 27 May 2026

Leung, D. M., Kok, J. F., Li, L., Lawrence, D. M., Mahowald, N. M., Tilmes, S., and Kluzek, E.: A global dust emission dataset for estimating dust radiative forcings in climate models, Atmos. Chem. Phys., 25, 2311–2331, https://doi.org/10.5194/acp-25-2311-2025, 2025.

Li, F., Vogelmann, A. M., & Ramanathan, V.: Saharan Dust Aerosol Radiative Forcing Measured from Space. J. Climate, 17, 2558–2571, https://doi.org/10.1175/1520-0442(2004)017<2558:SDARFM>2.0.CO;2, 2004.

Li, J., Carlson, B. E., Yung, Y. L., Lv, D., Hansen, J., Penner, J. E., Liao, H., Ramaswamy, V., Kahn, R. A., Zhang, P., Dubovik, O., Ding, A., Lacis, A. A., Zhang, L., and Dong, Y.: Scattering and absorbing aerosols in the climate system, Nat. Rev. Earth Environ., 3(6), 363–379, https://doi.org/10.1038/s43017-022-00296-7, 2022.

Li, L., Mahowald, N. M., Miller, R. L., Pérez García-Pando, C., Klose, M., Hamilton, D. S., Gonçalves Ageitos, M., Ginoux, P., Balkanski, Y., Green, R. O., Kalashnikova, O., Kok, J. F., Obiso, V., Paynter, D., and Thompson, D. R.: Quantifying the range of the dust direct radiative effect due to source mineralogy uncertainty, Atmos. Chem. Phys., 21, 3973–4005, https://doi.org/10.5194/acp-21-3973-2021, 2021.

Lian, L., Huang, J., Chen, S., Du, S., Zhang, L., & Yang, J.: A comprehensive review of dust events: characteristics, climate feedbacks, and public health risks. Current Pollution Reports, 11(1), 18, 2025.

Lohmann, U., & Feichter, J.: Can the direct and semi-direct aerosol effect compete with the indirect effect on a global scale?. Geophysical Research Letters, 28(1), 159-161, 2001.

Marinou, E., Amiridis, V., Binietoglou, I., Tsikerdekis, A., Solomos, S., Proestakis, E., Konsta, D., Papagiannopoulos, N., Tsekeri, A., Vlastou, G., Zanis, P., Balis, D., Wandinger, U., and Ansmann, A.: Three-dimensional evolution of Saharan dust transport towards Europe based on a 9-year EARLINET-optimized CALIPSO dataset, Atmos. Chem. Phys., 17, 5893–5919, https://doi.org/10.5194/acp-17-5893-2017, 2017.

Masoom, A., Fountoulakis, I., Kazadzis, S., Raptis, I.-P., Kampouri, A., Psiloglou, B. E., Kouklaki, D., Papachristopoulou, K., Marinou, E., Solomos, S., Gialitaki, A., Founda, D., Salamalikis, V., Kaskaoutis, D., Kouremeti, N., Mihalopoulos, N., Amiridis, V., Kazantzidis, A., Papayannis, A., Zerefos, C. S., and Eleftheratos, K.: Investigation of the effects of the Greek extreme wildfires of August 2021 on air quality and spectral solar irradiance, Atmos. Chem. Phys., 23, 8487–8514, https://doi.org/10.5194/acp-23-8487-2023, 2023.

Mateos, D., Toledano, C., Calle, A., Román, R., Herreras-Giralda, M., González, R., Herrero-Anta, S., González-Fernández, D., Herrero-del Barrio, C., Nisantzi, A., Mamouri, R. E., Groß, S., Cachorro, V. E., de Frutos, Á. M., and Weinzierl, B.: Saharan and Arabian dust optical properties registered by sun photometry during A-LIFE field experiment in Cyprus, Atmos. Chem. Phys., 26, 1993–2005, https://doi.org/10.5194/acp-26-1993-2026, 2026.

Mayer, B., Kylling, A.: Technical note: The libRadtran software package for radiative transfer calculations - description and examples of use. Atmos. Chem. Phys., 5(7), 1855–1877, 2005.

Meloni, D., di Sarra, A., Di Iorio, T., and Fiocco, G.: Direct radiative forcing of Saharan dust in the Mediterranean from measurements at Lampedusa Island and MISR space-borne observations, J. Geophys. Res., 109, D08206, https://doi.org/10.1029/2003JD003960, 2004.

https://doi.org/10.5194/egusphere-2026-2775
Preprint. Discussion started: 27 May 2026

Middleton, N. J.: Dust storms in the Middle East, J. Arid Environ., 10, 83–96, https://doi.org/10.1016/S0140-1963(86)80023-9, 1986.

Mlawer, E. J., and Clough, S. A.: Shortwave and longwave enhancements in the rapid radiative transfer model. Proc. Seventh Atmospheric Radiation Measurement (ARM) Science Team Meeting, San Antonio, TX, U.S. Dept. of Energy, 409– 413, 1998.

Mlawer, E.J., Iacono, M.J., Pincus, R., Barker, H.W., Oreopoulos, L., and Mitchell, D.L.: Contributions of the ARM Program to Radiative Transfer Modeling for Climate and Weather Applications, The Atmospheric Radiation Measurement Program: The First 20 Years, Meteor. Monograph, 57, Amer. Meteor. Soc., 2016.

Mlawer, E.J., Taubman, S. J., Brown, P. D., Iacono, M. J., and Clough, S. A.: Radiative transfer for inhomogeneous atmospheres: RRTM, a validated correlated-k model for the longwave. J. Geophys. Res., 102, 16 663–16 682, 1997.

Mok, J., Krotkov, N. A., Torres, O., Jethva, H., Li, Z., Kim, J., Koo, J.-H., Go, S., Irie, H., Labow, G., Eck, T. F., Holben, B. N., Herman, J., Loughman, R. P., Spinei, E., Lee, S. S., Khatri, P., and Campanelli, M.: Comparisons of spectral aerosol single scattering albedo in Seoul, South Korea, Atmos. Meas. Tech., 11, 2295–2311, https://doi.org/10.5194/amt-11-2295-2018, 2018.

Mona, L., Amiridis, V., Cuevas, E., Gkikas, A., Trippetta, S., Vandenbussche, S., Benedetti, A., Dagsson-Waldhauserova, P., Formenti, P., Haefele, A., Kazadzis, S., Knippertz, P., Laurent, B., Madonna, F., Nickovic, S., Papagiannopoulos, N., Pappalardo, G., Pérez García-Pando, C., Popp, T., Rodríguez, S., Sealy, A., Sugimoto, N., Terradellas, E., Vukovic Vimic, A., Weinzierl, B., & Basart, S.: Observing Mineral Dust in Northern Africa, the Middle East, and Europe: Current Capabilities and Challenges ahead for the Development of Dust Services. Bulletin of the American Meteorological Society, 104(12), E2223-E2264. https://doi.org/10.1175/BAMS-D-23-0005.1, 2023.

Monteiro, A., Basart, S., Kazadzis, S., Votsis, A., Gkikas, A., Vandenbussche, S., ... & Nickovic, S.: Multi-sectoral impact assessment of an extreme African dust episode in the Eastern Mediterranean in March 2018. Science of the Total Environment, 843, 156861, 2022.

Müller, B., Wild, M., Driesse, A., and Behrens, K.: Rethinking solar resource assessments in the context of global dimming and brightening, Sol. Energy, 99, 272–282, https://doi.org/10.1016/j.solener.2013.11.013, 2014.

Nabat, P., Somot, S., Mallet, M., Sevault, F., Chiacchio, M., and Wild, M.: Direct and semi-direct aerosol radiative effect on the Mediterranean climate variability using a regional climate system model, Clim. Dynam., 44, 1127–1155, https://doi.org/10.1007/s00382-014-2205-6, 2015.

Neher, I., Buchmann, T., Crewell, S., Pospichal, B., and Meilinger, S.: Impact of atmospheric aerosols on solar power, Meteorol. Z., 28(4), 305–321, https://doi.org/10.1127/metz/2019/0969, 2019.

Nickovic, S., Vukovic, A., and Vujadinovic, M.: Atmospheric processing of iron carried by mineral dust, Atmos. Chem. Phys., 13, 9169–9181, https://doi.org/10.5194/acp-13-9169-2013, 2013.

https://doi.org/10.5194/egusphere-2026-2775
Preprint. Discussion started: 27 May 2026

Nickovic, S., Vukovic, A., Vujadinovic, M., Djurdjevic, V., and Pejanovic, G.: Technical Note: High-resolution mineralogical database of dust-productive soils for atmospheric dust modeling, Atmos. Chem. Phys., 12, 845–855, https://doi.org/10.5194/acp-12-845-2012, 2012.

Papachristopoulou, K., Fountoulakis, I., Gkikas, A., Kosmopoulos, P. G., Nastos, P. T., Hatzaki, M., & Kazadzis, S.: 15-Year Analysis of Direct Effects of Total and Dust Aerosols in Solar Radiation/Energy over the Mediterranean Basin. Remote Sensing, 14(7), 1535. https://doi.org/10.3390/rs14071535, 2022.

Papachristopoulou, K., Fountoulakis, I., Gkikas, A., Kosmopoulos, P. G., Nastos, P. T., Hatzaki, M., and Kazadzis, S.: 15-year analysis of direct effects of total and dust aerosols in solar radiation/energy over the Mediterranean Basin, Remote Sens., 14(7), 1535, https://doi.org/10.3390/rs14071535, 2022.

Papadimitriou, N., Fountoulakis, I., Gkikas, A., Papachristopoulou, K., Kazantzidis, A., Kazadzis, S., Pfenninger, S., Kapsomenakis, J., Eleftheratos, K., Argiriou, A. A., Doppler, L., and Zerefos, C. S.: PV power modelling using solar radiation from ground-based measurements and CAMS: Assessing the diffuse component related uncertainties leveraging the Global Solar Energy Estimator (GSEE), Atmos. Meas. Tech., 19, 1227–1244, https://doi.org/10.5194/amt-19-1227-2026, 2026.

Papetta, A., Herrero del Barrio, C., Aslanoğlu, S. Y., Chadoulis, R.-T., Charalampous, G., Herrero-Anta, S., Kouklaki, D., Mytilinaios, M., Moustaka, A., Proestakis, E., Amiridis, V., Spyrou, C., Gkikas, A., Pikridas, M., Kezoudi, M., Marenco, F., Sciare, J., Vandenbussche, S., Solomos, S., Kazadzis, S., & Fountoulakis, I.: Source-dependent optical and mineral signatures of dust outbreaks over the Mediterranean. EGUsphere (preprint). Copernicus Publications, 2025.

Pappalardo, G., Amodeo, A., Apituley, A., Comeron, A., Freudenthaler, V., Linné, H., Ansmann, A., Bösenberg, J., D'Amico, G., Mattis, I., Mona, L., Wandinger, U., Amiridis, V., Alados-Arboledas, L., Nicolae, D., and Wiegner, M.: EARLINET: towards an advanced sustainable European aerosol lidar network, Atmos. Meas. Tech., 7, 2389–2409, https://doi.org/10.5194/amt-7-2389-2014, 2014.

Pérez, C., Nickovic, S., Pejanovic, G., Baldasano, J. M., and Özsoy, E.: Interactive dust-radiation modeling: A step to improve weather forecasts, J. Geophys. Res., 111, 1–17, 2006.

Pfenninger, S., & Staffell, I.: Long-term patterns of European PV output using 30 years of validated hourly reanalysis and satellite data. Energy, 114, 1251-1265, 2016.

Polo, J., and Estalayo, G.: Impact of atmospheric aerosol loads on concentrating solar power production in arid-desert sites, Sol. Energy, 115, 621–631, https://doi.org/10.1016/j.solener.2015.03.031, 2015.

Ramanathan, V. C. P. J., Crutzen, P. J., Kiehl, J. T., & Rosenfeld, D.: Aerosols, climate, and the hydrological cycle. science, 294(5549), 2119-2124, 2001.

Renard, J. B., et al.: In situ measurements of desert dust particles above the western Mediterranean Sea with the balloon-borne Light Optical Aerosol Counter/sizer (LOAC) during the ChArMEx campaign of summer 2013, Atmos. Chem. Phys., 18, 3677–3699, https://doi.org/10.5194/acp-18-3677-2018, 2018.

https://doi.org/10.5194/egusphere-2026-2775
Preprint. Discussion started: 27 May 2026

Rezvani, M., Gholami, A., Gavagsaz-Ghoachani, R., & Zandi, M.: A Review on The Effect of Dust Properties on Photovoltaic Solar Panels' Performance. Journal of Renewable and New Energy, 2023.

Riemer, N., Ault, A. P., West, M., Craig, R. L., and Curtis, J. H.: Aerosol mixing state: measurements, modeling, and impacts, Rev. Geophys., 57, 187–249, https://doi.org/10.1029/2018RG000607, 2019.

Rodríguez, S. and López-Darias, J.: Extreme Saharan dust events expand northward over the Atlantic and Europe, prompting record-breaking PM10 and PM2.5 episodes, Atmos. Chem. Phys., 24, 12031–12053, https://doi.org/10.5194/acp-24-12031-2024, 2024.

Rodríguez, S., Calzolai, G., Chiari, M., Nava, S., García, M. I., López-Solano, J., Marrero, C., López-Darias, J., Cuevas, E., Alonso-Pérez, S., Prats, N., Amato, F., Lucarelli, F., & Querol, X.: Rapid changes of dust geochemistry in the Saharan Air Layer linked to sources and meteorology. Atmospheric Environment, 223, 117186. https://doi.org/10.1016/j.atmosenv.2019.117186, 2020.

Ruckstuhl, C., Norris, J. R. and Philipona, R.: Is there evidence for an aerosol indirect effect during the recent aerosol optical depth decline in Europe? J. Geophys. Res., 115, D04204, doi:10.1029/2009JD012867, 2010.

Ruiz-Arias, J., Gueymard, C., Santos-Alamillos, F., et al.: Worldwide impact of aerosol's time scale on the predicted long-term concentrating solar power potential, Sci. Rep., 6, 30546, https://doi.org/10.1038/srep30546, 2016.

Samset, B. H., et al.: Aerosol absorption: progress towards global and regional constraints, Curr. Clim. Change Rep., 4, 65–83, https://doi.org/10.1007/s40641-018-00028-7, 2018.

Schwander, H., Koepke, P. and Ruggaber, A.: Uncertainties in modeled UV irradiances due to limited accuracy and availability of input data, J. Geophys. Res., 102(D8), 9419–9429, doi:10.1029/97JD00244, 1997.

Seinfeld, J. H., et al.: ACE-ASIA — regional climatic and atmospheric chemical effects of Asian dust and pollution, Bull. Am. Meteorol. Soc., 85, 367–380, https://doi.org/10.1175/BAMS-85-3-367, 2004.

Senthilarasu, S., Fernández, E. F., Almonacid, F., & Mallick, T. K.: Effects of spectral coupling on perovskite solar cells under diverse climatic conditions. Solar Energy Materials and Solar Cells, 133, 92–98. https://doi.org/10.1016/j.solmat.2014.10.037, 2015.

Sepúlveda-Oviedo, E. H.: A review of operational factors affecting photovoltaic system performance. Energy Conversion and Management: X, 26, 100942, 2025.

Sinyuk, A., Holben, B. N., Eck, T. F., Giles, D. M., Slutsker, I., Korkin, S., Schafer, J. S., Smirnov, A., Sorokin, M., and Lyapustin, A.: The AERONET Version 3 aerosol retrieval algorithm, associated uncertainties and comparisons to Version 2, Atmos. Meas. Tech., 13, 3375–3411, https://doi.org/10.5194/amt-13-3375-2020, 2020.

Sokolik, I. N., and Toon, O. B.: Incorporation of mineralogical composition into models of the radiative properties of mineral aerosol from UV to IR wavelengths, J. Geophys. Res. Atmos., 104, 9423–9444, https://doi.org/10.1029/1999JD900051, 1999.

https://doi.org/10.5194/egusphere-2026-2775
Preprint. Discussion started: 27 May 2026

Solomos, S., Spyrou, C., Barreto, A., Rodríguez, S., González, Y., Neophytou, M. K., Zerefos, C.: The development of METAL-WRF Regional Model for the Description of Dust Mineralogy in the Atmosphere, Atmosphere, 14, 1615, https://doi.org/10.3390/atmos14111615, 2023.

Spyrou, C., Fountoulakis, I., Solomos, S., Papadimitriou, N., Bais, A., Groebner, J., Meloni, D., and Zerefos, C.: Implications of dust minerals on radiative transfer at regional scale, using the METAL-WRF model, EGUsphere [preprint], https://doi.org/10.5194/egusphere-2025-3570, 2025.

Stamnes, K., Tsay, S., Wiscombe, W., and Jayaweera, K.: A numerically stable algorithm for discrete-ordinate-method radiative transfer in multiple scattering and emitting layered media, Appl. Opt., 27, 2502–2509, 1988.

Stamnes, K., Tsay, S.-C., Wiscombe, W., and Laszlo, I.: DISORT, a General-Purpose Fortran Program for Discrete-Ordinate-Method Radiative Transfer in Scattering and Emitting Layered Media: Documentation of Methodology, Dept. of Physics and Engineering Physics, Stevens Institute of Technology, Hoboken, 2000.

Stein, A. F., Draxler, R. R., Rolph, G. D., Stunder, B. J. B., Cohen, M. D., & Ngan, F.: NOAA's HYSPLIT Atmospheric Transport and Dispersion Modeling System. Bulletin of the American Meteorological Society, 96(12), 2059-2077. https://doi.org/10.1175/BAMS-D-14-00110.1, 2015.

Teri, M., Gasteiger, J., Heimerl, K., Dollner, M., Schöberl, M., Seibert, P., Tipka, A., Müller, T., Aryasree, S., Kandler, K., and Weinzierl, B.: Pollution affects Arabian and Saharan dust optical properties in the eastern Mediterranean, Atmos. Chem. Phys., 25, 6633–6662, https://doi.org/10.5194/acp-25-6633-2025, 2025.

Thevenard, D., & Pelland, S.: Estimating the uncertainty in long-term photovoltaic yield predictions. Solar energy, 91, 432-445, 2013.

Twomey, S.: Aerosols, clouds and radiation. Atmospheric Environment. Part A. General Topics, 25(11), 2435-2442, 1991.

Uno, I., Eguchi, K., Yumimoto, K. et al. Asian dust transported one full circuit around the globe. Nature Geosci 2, 557–560. https://doi.org/10.1038/ngeo583, 2009.

Varga, G., Gresina, F., Gelencsér, A., Csávics, A., & Rostási, Á.: The shadow of the wind: The impact of Saharan dust on photovoltaic power generation in the Mediterranean. Renewable Energy, 256(Part F), 124337. https://doi.org/10.1016/j.renene.2025.124337, 2026.

Warren, A., Chappell, A., Todd, M. C., Bristow, C., Drake, N., Engelstaedter, S., Washington, R.: Dust-raising in the dustiest place on earth, Geomorphology, 92, 25–37, https://doi.org/10.1016/j.geomorph.2007.04.006, 2007.

Weihs, P., and Webb, A. R.: Accuracy of spectral UV model calculations: 1. Consideration of uncertainties in input parameters, J. Geophys. Res., 102(D1), 1541–1550, doi:10.1029/96JD01242, 1997.

Wild, M.: Global Dimming/Brightening. In International Encyclopedia of Geography: People, the Earth, Environment and Technology (eds D. Richardson, N. Castree, M.F. Goodchild, A. Kobayashi, W. Liu and R.A. Marston). https://doi.org/10.1002/9781118786352.wbieg0176, 2017.